J. Fluid Mech. (2005), *vol.* 533, *pp.* 193–221.
doi:10.1017/S0022112005004349 Printed in the United Kingdom

Surface-tension-driven flow outside a slender wedge with an application to the inviscid coalescence of drops

By J. BILLINGHAM[1] AND A. C. KING[2,3]†

[1]School of Mathematical Sciences, The University of Nottingham, University Park, Nottingham, NG7 2RD, UK

[2]School of Mathematics and Statistics, The University of Birmingham, Edgbaston, Birmingham, B15 2TT, UK

[3]Department of Mathematics, The University of Reading, Whiteknights, Reading, RG6 6AX, UK

(Received 15 June 2004 and in revised form 4 January 2005)

We consider the two-dimensional inviscid flow that occurs when a fluid, initially at rest around a slender wedge-shaped void, is allowed to recoil under the action of surface tension. As noted by Keller & Miksis (1983), a similarity scaling is available, with lengths scaling like $t^{2/3}$. We find that an asymptotic balance is possible when the wedge semi-angle, α, is small, in an inner region of $O(\alpha^{4/9})$, a distance of $O(\alpha^{-2/9})$ from the origin, which leads to a simpler boundary value problem at leading order. Although we are able to reformulate the inner problem in terms of a complex potential and reduce it to a single nonlinear integral equation, we are unable to find a solution numerically. This is because, as noted by Vanden-Broeck, Keller & Milewski (2000), and reproduced here numerically using a boundary integral method, the free surface is self-intersecting for $\alpha < \alpha_0 \approx 2.87^\circ$. Since disconnected solutions are only possible when there is a void inside the initial wedge, we consider the effect of an inviscid low-density fluid inside the wedge. In this case, a solution is available for a slightly smaller range of wedge semi-angles, since the flow of the interior fluid sucks the free surfaces together, with the exterior flow seeing pinch-off at a finite angle.

We conclude that for $\alpha < \alpha_0$, we must introduce the effect of viscosity at small times in order to regularize the initial value problem. Since the solution for $t \ll 1$ in the presence of viscosity is simply connected (Billingham 2005), the free surface must first pinch off at some finite time and then continue to do so at a sequence of later times. We investigate this using boundary integral solutions of the full inviscid initial value problem, with smooth initial conditions close to those of the original problem. In addition, we show that the inner asymptotic scalings that we developed for the steady problem can also be used in this time-dependent problem. The unsteady inner equations reduce to those for steady unidirectional flow outside a region of constant pressure, and can be solved numerically.

We also show how the slender wedge solution can be related to the small-time behaviour of two coalescing drops, and describe the relationship between our solutions and those found by Duchemin, Eggers & Josserand (2003), for which a similar unsteady inner region exists. In each case, the free surface pinches off repeatedly, and no similarity solution exists.

---

† Professor King died in January 2005.

1. Introduction

Inviscid surface-tension-driven flow in a fluid wedge was first studied by Keller & Miksis (1983), who noted that a similarity solution, with lengths scaling like $t^{2/3}$, is available. These scalings have since been used by many other authors to study related problems, for example, Lawrie (1990), Lawrie & King (1991), King (1991), Billingham & King (1995), King, Billingham & Popple (1999), Billingham (1999), Decent & King (2001), Keller, Milewski & Vanden-Broeck (2000, 2002), Sierou & Lister (2004). Such flows are relevant to situations where bodies of fluid rupture and recoil under the action of surface tension. As we show below, we can also relate the surface-tension-driven flow around a wedge to the behaviour of two coalescing liquid spheres or cylinders (Duchemin, Eggers & Josserand 2003).

In this paper, we consider the flow of two immiscible fluids, initially lying in the exterior and interior of a single wedge. We concentrate on the behaviour when the interior fluid either has zero density or density much smaller than the exterior fluid, and the wedge angle is small; a slender wedge. We begin in § 2 by defining the initial value problem and determine the boundary value problem satisfied by the similarity solution. In § 2.1, we construct asymptotic scalings for an inner and an outer solution, valid when the wedge angle is small. We show that, although this structure is plausible, no solution exists in the inner region. We show why this is the case in § 2.2, where we solve the similarity problem numerically, and find that simply connected solutions only exist for sufficiently large wedge angles. The free surface becomes self-intersecting at small wedge angles because of the presence of large-amplitude capillary waves on the free surface, and therefore a similarity solution cannot exist for arbitrarily small wedge angles.

We consider the effect of an interior fluid with small, but non-zero, density in § 2.3. We find that the flow of the exterior fluid is only affected close to the point where a thin neck is formed in the interior fluid. However, we are again unable to find a solution of the inner problem in the slender wedge limit. Numerical solutions of the similarity problem show that there is still no solution for sufficiently small wedge angles, again because of the presence of large-amplitude capillary waves of the free surface. However, there is some numerical evidence that a similarity solution exists for all wedge angles when the inner fluid is moderately dense compared to the outer fluid.

In § 3, we further investigate the solution of the initial value problem for wedge angles small enough that no similarity solution exists. Unsteady numerical solutions, starting from smooth initial conditions, such as could emerge from the initial viscous-dominated flow, show that the similarity solution is an attractor for the unsteady flow when such a solution exists, but that otherwise the free surface pinches off a bubble in finite time. We show that the asymptotic scalings that we developed for the similarity problem can be used for the unsteady problem, after scaling time appropriately, in § 3.2. Numerical solutions of this unsteady inner problem are in good qualitative agreement with solutions of the full unsteady problem.

Finally, in § 4, we show how the unsteady inner solutions we have developed can be related to the inviscid coalescence of drops, as studied by Duchemin *et al.* (2003). Specifically, we find that there is a one-parameter family of scalings appropriate to an unsteady inner region, within which the free surface pinches off in finite time. The appropriate parameter is determined by matching to an outer solution, with different outer solutions appropriate for an initial wedge, the main subject of the present paper, and an initially quadratic free surface, the subject of Duchemin *et al.* (2003) as a model for the coalescence of two cylinders of fluid. It can be shown that this is

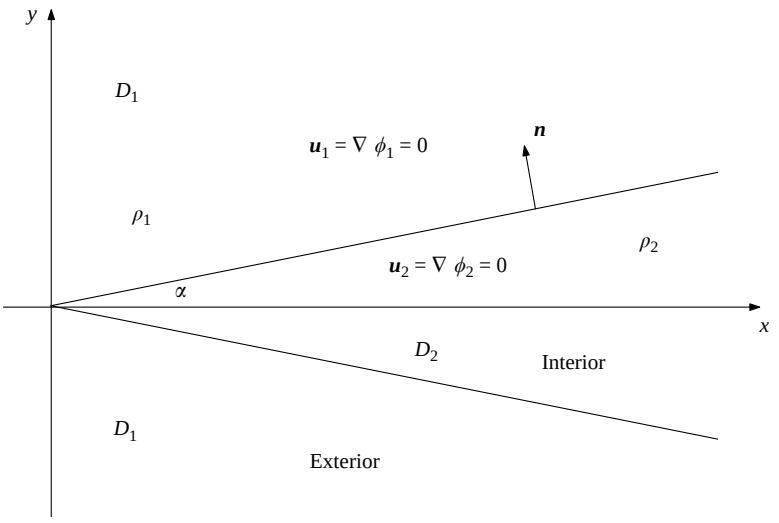

FIGURE 1. The initial conditions.

equivalent to the coalescence of three-dimensional droplets. In both cases, this means that there is no similarity solution; instead the free surface pinches off repeatedly.

2. Similarity solution of the initial value problem

We consider a two-dimensional flow involving two inviscid fluids, one of density ρ_2 initially at rest lying inside a wedge of semi-angle α, surrounded by a fluid of density ρ_1, also initially at rest, as shown in figure 1. The x-axis is a line of symmetry, and we will consider the region $y \geqslant 0$ only. We denote the domains occupied by fluids 1 and 2 by $D_{1,2}$. A constant, uniform surface tension, σ, acts at the interface between the two fluids, ∂D, and causes it to recoil for $t > 0$. Since the flow is initially irrotational, it remains irrotational, and we can describe the flow in each fluid using velocity potentials $\phi_{1,2}$, with the fluid velocities given by $\boldsymbol{u}_{1,2} = \nabla\phi_{1,2}$.

The potentials both satisfy Laplace's equation

$$\nabla^2\phi_{1,2} = 0 \quad \text{in } D_{1,2}. \tag{1}$$

If we describe the interface parametrically as $\boldsymbol{R} = (X(s,t), Y(s,t))$, where s is arc-length, then

$$X_s^2 + Y_s^2 = 1, \tag{2}$$

and we can write the dynamic boundary condition as

$$\rho_1\left(\phi_{1t} + \tfrac{1}{2}|\nabla\phi_1|^2\right) - \rho_2\left(\phi_{2t} + \tfrac{1}{2}|\nabla\phi_2|^2\right) = \sigma\kappa \equiv \sigma\left(-Y_{ss}X_s + X_{ss}Y_s\right) \quad \text{on } \partial D, \tag{3}$$

where κ is the curvature. The kinematic condition is

$$\boldsymbol{R}_t = \boldsymbol{n}\{\boldsymbol{n}\cdot\nabla\phi_1(\boldsymbol{R},t)\}, \tag{4}$$

where $\boldsymbol{n} = (-Y_s, X_s)$ is the unit normal pointing into D_1. Continuity of normal velocity requires that

$$\boldsymbol{n}\cdot\nabla\phi_1(\boldsymbol{R},t) = \boldsymbol{n}\cdot\nabla\phi_2(\boldsymbol{R},t). \tag{5}$$

Appropriate symmetry conditions are

$$\left.\begin{aligned} &Y_s(0,t)=1, \quad X_s(0,t)=0, \\ &\phi_{y1}(x,0,t)=0 \quad \text{for } t>0,\ x\leqslant X_0(t), \\ &\phi_{y2}(x,0,t)=0 \quad \text{for } t>0,\ x\geqslant X_0(t), \end{aligned}\right\} \tag{6}$$

and we define s so that $Y(0,t)=0$ and $X(0,t)\equiv X_0(t)$. The inital conditions are

$$\phi_{1,2}=0 \quad \text{in } D_{1,2}, \quad Y(s,0)=s\sin\alpha, \quad X(s,0)=s\cos\alpha. \tag{7}$$

In the far field

$$\phi_{1,2}\to 0 \quad \text{as } x^2+y^2\to\infty, \quad Y-\tan\alpha\ X\to 0 \quad \text{as } s\to\infty. \tag{8}$$

There is no geometrical lengthscale in this problem, and the only dimensional quantities involved are $\rho_{1,2}$ and σ. As noted by Keller & Miksis (1983), we can therefore define the independent similarity variables

$$\bar{x}=\frac{\rho_1^{1/3}x}{\sigma^{1/3}t^{2/3}}, \quad \bar{y}=\frac{\rho_1^{1/3}y}{\sigma^{1/3}t^{2/3}}, \quad \bar{s}=\frac{\rho_1^{1/3}s}{\sigma^{1/3}t^{2/3}}, \tag{9}$$

and look for a solution of the form

$$\bar{\phi}_{1,2}=\frac{\rho_1^{2/3}\phi_{1,2}}{\sigma^{2/3}t^{1/3}}\equiv\bar{\phi}_{1,2}(\bar{x},\bar{y}), \quad \bar{Y}=\frac{\rho_1^{1/3}Y}{\sigma^{1/3}t^{2/3}}\equiv\bar{Y}(\bar{s}), \quad \bar{X}=\frac{\rho_1^{1/3}X}{\sigma^{1/3}t^{2/3}}\equiv\bar{X}(\bar{s}). \tag{10}$$

In terms of these similarity variables, the initial value problem (1) to (8) becomes the boundary value problem

$$\nabla^2\bar{\phi}_{1,2}=0 \quad \text{in } D_{1,2}, \tag{11}$$

$$\bar{X}_{\bar{s}}^2+\bar{Y}_{\bar{s}}^2=1, \tag{12}$$

$$\tfrac{1}{3}\bar{\phi}_1-\tfrac{2}{3}\bar{\boldsymbol{R}}\cdot\nabla\bar{\phi}_1+\tfrac{1}{2}|\nabla\bar{\phi}_1|^2-\rho\left\{\tfrac{1}{3}\bar{\phi}_2-\tfrac{2}{3}\bar{\boldsymbol{R}}\cdot\nabla\bar{\phi}_2+\tfrac{1}{2}|\nabla\bar{\phi}_2|^2\right\}$$
$$=-\bar{Y}_{\bar{s}\bar{s}}\bar{X}_{\bar{s}}+\bar{X}_{\bar{s}\bar{s}}\bar{Y}_{\bar{s}} \quad \text{on } \partial D, \tag{13}$$

$$\tfrac{2}{3}\bar{\boldsymbol{n}}\cdot\bar{\boldsymbol{R}}=\bar{\boldsymbol{n}}\cdot\nabla\bar{\phi}_1=\bar{\boldsymbol{n}}\cdot\nabla\bar{\phi}_2 \quad \text{on } \partial D, \tag{14}$$

$$\bar{Y}_s(0)=1, \quad \bar{X}(0)=0, \quad \bar{\phi}_{\bar{y}1}(\bar{x},0)=0 \quad \text{for } \bar{x}\leqslant\bar{X}_0, \quad \bar{\phi}_{\bar{y}2}(\bar{x},0)=0 \quad \text{for } \bar{x}\geqslant\bar{X}_0, \tag{15}$$

$$\bar{\phi}_{1,2}\to 0 \quad \text{as } \bar{x}^2+\bar{y}^2\to\infty, \qquad \bar{Y}-\tan\alpha\ \bar{X}\to 0 \quad \text{as } \bar{s}\to\infty, \tag{16}$$

where $\rho=\rho_2/\rho_1$.

We shall begin by considering the case of a void in D_2, so that $\rho=0$. To keep our notation succinct, we write $\phi=\bar{\phi}_1$, $D=D_1$, $\tan\alpha=\epsilon$ and omit the bars from the variables. We also write $\Phi(s)=\phi(X(s),Y(s))$ and use (14) to eliminate $\boldsymbol{n}\cdot\nabla\phi(X(s),Y(s))\equiv\Phi_n(s)$ from (13), which gives

$$\nabla^2\phi=0 \quad \text{in } D, \tag{17}$$

$$X'^2+Y'^2=1, \tag{18}$$

$$\tfrac{1}{3}\Phi-\tfrac{2}{9}(\boldsymbol{n}\cdot\boldsymbol{R})^2-\tfrac{2}{3}(\boldsymbol{t}\cdot\boldsymbol{R})\Phi'+\tfrac{1}{2}(\Phi')^2=-Y''X'+X''Y', \tag{19}$$

$$\Phi_n=\tfrac{2}{3}\boldsymbol{n}\cdot\boldsymbol{R}, \tag{20}$$

$$Y'(0)=1, \quad X'(0)=0, \tag{21}$$

$$\phi_y(x,0)=0 \quad \text{for } x<X_0, \tag{22}$$

$$\phi\to 0 \quad \text{as } x^2+y^2\to\infty, \qquad Y-\epsilon X\to 0 \quad \text{as } s\to\infty, \tag{23}$$

where $\boldsymbol{t} = (X', Y')$ is the unit tangent vector in the direction of increasing s and a prime denotes $\mathrm{d}/\mathrm{d}s$.

2.1. *The slender wedge limit, $\epsilon \ll 1$*

We begin by seeking an asymptotic solution of (17) to (23), valid when $\epsilon \ll 1$; the slender wedge limit. By looking for an asymptotic balance in the equations, we are led to seek a solution in an outer region with $x, y = O(\epsilon^{-a})$, $Y = O(\epsilon^{1-a})$ and $\phi = O(\epsilon^{1-2a})$. By considering how the solution in this outer region behaves as $x \to \bar{X}_0\epsilon^{-a}$, where the free surface meets the x-axis, we find that $\bar{Y} = O((\bar{x} - \bar{X}_0)^{-1/2}) + O(\epsilon^{3a}(\bar{x} - \bar{X}_0)^{-3/2})$ as $\bar{x} \to \bar{X}_0$, with $\bar{x} = \epsilon^a x$ and $\bar{Y} = \epsilon^{a-1} Y$. This suggests a non-uniformity when $\bar{x} = \bar{X}_0 + O(\epsilon^{3a})$. In addition, the curvature is proportional to $\bar{Y}_{\bar{x}\bar{x}}(1 + \epsilon^2 \bar{Y}_{\bar{x}}^2)^{-3/2}$, so that, in order to obtain the full curvature term in an inner region, we need $\bar{x} = \bar{X}_0 + O(\epsilon^{2/3})$, and hence $a = 2/9$. We will describe the solutions in the inner and outer regions using $a = 2/9$ from the outset.

2.1.1. *Outer problem*

Appropriate scaled variables for the outer region are

$$\left.\begin{array}{llll} x = \epsilon^{-2/9}\bar{x}, & y = \epsilon^{-2/9}\bar{y}, & X = \epsilon^{-2/9}\bar{X}, & Y = \epsilon^{7/9}\bar{Y}, \\ s = \epsilon^{-2/9}\bar{s}, & \phi = \epsilon^{5/9}\bar{\phi}, & \Phi = \epsilon^{5/9}\bar{\phi}, & \Phi_n = \epsilon^{7/9}\bar{\phi}_n. \end{array}\right\} \tag{24}$$

At leading order for $\epsilon \ll 1$, (17) to (23) become

$$\nabla^2\bar{\phi} = 0 \quad \text{for } \bar{y} > 0, \tag{25}$$

$$\bar{X}'^2 = 1, \tag{26}$$

$$\tfrac{1}{3}\bar{\Phi} - \tfrac{2}{3}\bar{X}\bar{\Phi}' = 0, \tag{27}$$

$$\bar{\Phi}_n = \bar{\phi}_{\bar{y}}(\bar{x}, 0) = \tfrac{2}{3}(\bar{X}'\bar{Y} - \bar{Y}'\bar{X}) \quad \text{for } \bar{x} > \bar{X}_0, \tag{28}$$

$$\bar{\phi}_{\bar{y}}(\bar{x}, 0) = 0 \quad \text{for } \bar{x} < \bar{X}_0, \tag{29}$$

$$\bar{\phi} \to 0 \quad \text{as } \bar{x}^2 + \bar{y}^2 \to \infty, \quad \bar{Y} - \bar{X} \to 0 \quad \text{as } s \to \infty. \tag{30}$$

Note that the symmetry condition, (21), will be satisfied by the free surface in the inner region, and that surface tension does not affect the flow at leading order in this outer region.

Equation (26) shows that $\bar{X} = \bar{X}_0 + \bar{s}$, after which we can solve (27) to give $\bar{\Phi} = k\sqrt{\bar{s} + \bar{X}_0}$ for some constant k. The far-field condition (30) then shows that we need $k = 0$, and hence that, at leading order,

$$\bar{\phi}(\bar{x}, 0) = 0 \quad \text{for } \bar{x} > \bar{X}_0. \tag{31}$$

The least singular solution of (25) that satisfies (29), (30) and (31) is

$$\bar{\phi} = A\frac{\sin\frac{1}{2}\theta}{\bar{r}^{1/2}}, \tag{32}$$

where $(\bar{r}, \theta)$ are polar coordinates with origin at $\bar{x} = \bar{X}_0$, $\bar{y} = 0$ and A is a constant. On substituting this expression into the kinematic condition, (28), we can solve for the position of the free surface as

$$\begin{aligned} \bar{Y} &= \bar{x} + \frac{3}{4}A\int_{\bar{x}}^{\infty} \frac{\mathrm{d}s}{s^2(s - \bar{X}_0)^{3/2}} \\ &= \bar{x} + \frac{3A}{2\bar{X}_0^{5/2}}\bar{x}\left[\frac{3}{2}\left\{\tan^{-1}\left(\sqrt{\frac{\bar{x} - \bar{X}_0}{\bar{X}_0}}\right) - \frac{\pi}{2}\right\} + \frac{\bar{X}_0^{3/2}(\bar{x} - \bar{X}_0)^{1/2}}{2\bar{x}^2} + \sqrt{\frac{\bar{X}_0}{\bar{x} - \bar{X}_0}}\right]. \end{aligned} \tag{33}$$

We can see from this that

$$\bar{Y} \sim \frac{3A}{2\bar{X}_0}(\bar{x} - \bar{X}_0)^{-1/2} \quad \text{as } \bar{x} \to \bar{X}_0. \tag{34}$$

This singularity indicates that we need to scale into an inner region where the distance of the free surface from the y-axis is asymptotically larger than in the outer region, and surface tension is active at leading order.

2.1.2. *Inner problem*

Appropriate scaled variables for the inner region are

$$\left.\begin{aligned} &x - \epsilon^{-2/9}\bar{X}_0 - \epsilon^{4/9}\tilde{X}_0 = \epsilon^{4/9}\tilde{x}, \quad y = \epsilon^{4/9}\tilde{y}, \quad X - \epsilon^{-2/9}\bar{X}_0 - \epsilon^{4/9}\tilde{X}_0 = \epsilon^{4/9}\tilde{X}, \\ &Y = \epsilon^{4/9}\tilde{Y}, \quad s = \epsilon^{4/9}\tilde{s}, \quad \phi = \epsilon^{2/9}\tilde{\phi}, \quad \Phi = \epsilon^{2/9}\tilde{\Phi}, \quad \Phi_n = \epsilon^{-2/9}\tilde{\Phi}_n. \end{aligned}\right\} \tag{35}$$

The free surface meets the x-axis at $x = \epsilon^{-2/9}\bar{X}_0 + \epsilon^{4/9}\tilde{X}_0 + o(\epsilon^{4/9})$. The constant $\tilde{X}_0$ is determined by the solution at higher order, and we will not consider it further here. At leading order for $\epsilon \ll 1$, (17) to (22) become

$$\nabla^2\tilde{\phi} = 0 \quad \text{for } \tilde{y} > \tilde{Y},\ \tilde{x} > 0 \text{ and for } \tilde{y} > 0,\ \tilde{x} < 0, \tag{36}$$

$$\tilde{X}'^2 + \tilde{Y}'^2 = 1, \tag{37}$$

$$-\tfrac{2}{9}\bar{X}_0^2\tilde{Y}'^2 - \tfrac{2}{3}\bar{X}_0\tilde{X}'\tilde{\Phi}' + \tfrac{1}{2}(\tilde{\Phi}')^2 = -\tilde{Y}''\tilde{X}' + \tilde{X}''\tilde{Y}', \tag{38}$$

$$\tilde{\Phi}_n = -\tilde{Y}'\tilde{\phi}_{\tilde{x}} + \tilde{X}'\tilde{\phi}_{\tilde{y}} = -\tfrac{2}{3}\bar{X}_0\tilde{Y}', \tag{39}$$

$$\tilde{Y}'(0) = 1, \quad \tilde{X}'(0) = 0, \tag{40}$$

$$\tilde{\phi}_{\tilde{y}}(\tilde{x}, 0) = 0 \quad \text{for } \tilde{x} < 0. \tag{41}$$

Matching with the outer solution gives the far-field conditions

$$\tilde{Y} \sim \frac{A}{\bar{X}_0\tilde{X}^{1/2}} \quad \text{as } \tilde{s} \to \infty, \tag{42}$$

$$\tilde{\phi} \sim A\frac{\sin\frac{1}{2}\theta}{\tilde{r}^{1/2}} \quad \text{as } \tilde{r} \to \infty, \tag{43}$$

where $(\tilde{r}, \theta)$ are polar coordinates centred at the origin of the inner region.

After making use of (37), we note that (38) and (39) can be written as

$$\tfrac{1}{2}\left(\tilde{\Phi}' - \tfrac{2}{3}\bar{X}_0\tilde{X}'\right)^2 - \tfrac{2}{9}\bar{X}_0^2 = -\tilde{Y}''\tilde{X}' + \tilde{X}''\tilde{Y}', \quad -\tilde{Y}'\left(\tilde{\phi} - \tfrac{2}{3}\bar{X}_0\tilde{x}\right)_{\tilde{x}} + \tilde{X}'\tilde{\phi}_{\tilde{y}} = 0.$$

This suggests the change of variables

$$\left.\begin{aligned} &\tilde{x} = \bar{X}_0^{-2}\hat{x}, \quad \tilde{y} = \bar{X}_0^{-2}\hat{y}, \quad \tilde{X} = \bar{X}_0^{-2}\hat{X}, \quad \tilde{Y} = \bar{X}_0^{-2}\hat{Y}, \\ &\tilde{s} = \bar{X}_0^{-2}\hat{s}, \quad \tilde{\phi} = \tfrac{2}{3}\bar{X}_0\tilde{x} + \bar{X}_0^{-1}\hat{\phi}, \quad \tilde{\Phi} = \tfrac{2}{3}\bar{X}_0\tilde{X} + \bar{X}_0^{-1}\hat{\Phi}, \quad \tilde{\Phi}_n = \bar{X}_0\hat{\Phi}_n, \end{aligned}\right\} \tag{44}$$

in terms of which the problem becomes

$$\nabla^2\hat{\phi} = 0 \quad \text{for } \hat{y} > \hat{Y},\ \hat{x} > 0 \text{ and for } \hat{y} > 0,\ \hat{x} < 0, \tag{45}$$

$$\hat{X}'^2 + \hat{Y}'^2 = 1, \tag{46}$$

$$\tfrac{1}{2}(\hat{\Phi}')^2 - \tfrac{2}{9} = -\hat{Y}''\hat{X}' + \hat{X}''\hat{Y}', \tag{47}$$

$$\hat{\Phi}_n = -\hat{Y}'\hat{\phi}_{\hat{x}} + \hat{X}'\hat{\phi}_{\hat{y}} = 0, \tag{48}$$

$$\hat{Y}'(0) = 1, \quad \hat{X}'(0) = 0, \tag{49}$$

$$\hat{\phi}_{\hat{y}}(\hat{x}, 0) = 0 \quad \text{for } \hat{x} < 0, \tag{50}$$

$$\hat{Y} \sim \frac{A\bar{X}_0^2}{\bar{X}_0 \hat{X}^{1/2}} \quad \text{as } \hat{s} \to \infty, \tag{51}$$

$$\hat{\phi} \sim -\tfrac{2}{3}\hat{x} + A\bar{X}_0^2 \frac{\sin \frac{1}{2}\theta}{\hat{r}^{1/2}} \quad \text{as } \hat{r} \to \infty. \tag{52}$$

In this manner, we have transformed the inner problem into that of steady flow around a region of constant pressure, with a uniform velocity in the negative x-direction of size $\frac{2}{3}$ in the far field. This problem can be reformulated as an integral equation using a complex variable method, as used by Crapper (1957) to find an analytical solution for capillary waves.

We write the complex potential as $w = \phi + \mathrm{i}\psi$, where ψ is the stream function, dropping the hats on the variables for the moment. Since ϕ and ψ satisfy the Cauchy–Riemann equations, w is an analytic function of $z = x + \mathrm{i}y$ provided w is sufficiently smooth. In addition,

$$\frac{\mathrm{d}w}{\mathrm{d}z} = \phi_x + \mathrm{i}\psi_x = u - \mathrm{i}v \equiv q\mathrm{e}^{-\mathrm{i}\theta},$$

where q is the speed of the fluid and θ the angle the flow makes with the x-axis. We now write

$$\log\left(\frac{\mathrm{d}w}{\mathrm{d}z}\right) = \log q - \mathrm{i}\theta \equiv \tau - \mathrm{i}\theta.$$

Since $\tau \equiv \log q$ is an analytic function of $w = \phi + \mathrm{i}\psi$, except at stagnation points, τ is a harmonic function of ϕ and ψ. We note that

$$\kappa \equiv -\theta_s = -q\theta_\phi = -q\tau_\psi,$$

which allows us to write the boundary value problem (45) to (52) as

$$\tau_{\phi\phi} + \tau_{\psi\psi} = 0 \quad \text{for } \psi > 0, -\infty < \phi < \infty, \tag{53}$$

subject to

$$\tau_\psi = \begin{cases} 0 & \text{on } \psi = 0 \text{ for } \phi > 0, \\ \frac{2}{9}\mathrm{e}^{-\tau} - \frac{1}{2}\mathrm{e}^{\tau} & \text{on } \psi = 0 \text{ for } \phi < 0, \end{cases} \tag{54}$$

$$\tau \to \log\left(\frac{2}{3}\right) \quad \text{as } \phi^2 + \psi^2 \to \infty. \tag{55}$$

The simple redefinition $\tau = \log(2/3) + \hat{\tau}$ gives the more useful form

$$\hat{\tau}_{\phi\phi} + \hat{\tau}_{\psi\psi} = 0 \quad \text{for } \psi > 0, -\infty < \phi < \infty, \tag{56}$$

subject to

$$\hat{\tau}_\psi = \begin{cases} 0 & \text{on } \psi = 0 \text{ for } \phi > 0, \\ -\frac{2}{3}\sinh\hat{\tau} & \text{on } \psi = 0 \text{ for } \phi < 0, \end{cases} \tag{57}$$

$$\hat{\tau} \to 0 \quad \text{as } \phi^2 + \psi^2 \to \infty. \tag{58}$$

Finally, since we know that there must be a stagnation point where the free surface meets the x-axis, we must also enforce

$$\hat{\tau} \sim \tfrac{1}{2}\log|\phi| \quad \text{as } \phi \to 0 \quad \text{on } \psi = 0. \tag{59}$$

We can reformulate this as the single integral equation,

$$\hat{\tau}(\phi, 0) = \tfrac{1}{2}\log|\phi| - \frac{2}{3\pi}\int_{-\infty}^{0} \sinh\hat{\tau}(\xi, 0)\,\log|\xi - \phi|\,\mathrm{d}\xi. \tag{60}$$

We have thereby reduced the free boundary problem that we started with to a nonlinear integral equation. It is straightforward to discretize this equation, using the trapezium rule to evaluate the integral after subtracting out the integrable singularities in the integrand at $\xi = 0$ and $\xi = \phi$. However, we have been unable to compute a solution of (60), despite trying a variety of continuation methods and different ways of approximating the integral. Although we do not have a rigorous proof that (60) has no solution, the results that we present in the next section show that there is a good reason to expect that no solution exists.

2.2. *Numerical solution*

Having failed to find a solution for $\epsilon \ll 1$, we can investigate the reasons for this by solving the full problem, (17) to (23), numerically. It is convenient to use a boundary integral formulation of the problem. Specifically, we can replace (17) and (20) with

$$\Phi(s_0) = \frac{1}{\pi}\int_{-\infty}^{\infty}\left[\tfrac{2}{3}\{\boldsymbol{n}(s)\cdot\boldsymbol{R}(s)\}\log r + \frac{\boldsymbol{n}(s)\cdot\{\boldsymbol{R}(s_0)-\boldsymbol{R}(s)\}}{r^2}\Phi(s)\right]\mathrm{d}s, \tag{61}$$

where $r = |\boldsymbol{R}(s) - \boldsymbol{R}(s_0)|$ and $\boldsymbol{n}(s) = (-Y'(s), X'(s))$. We can also use the symmetry of the solution about the x-axis to reduce the domain of integration to $s \geqslant 0$, with

$$\Phi(s_0) = \frac{1}{\pi}\int_{0}^{\infty}\left[\tfrac{2}{3}\{\boldsymbol{n}(s)\cdot\boldsymbol{R}(s)\}\log r + \frac{\boldsymbol{n}(s)\cdot\{\boldsymbol{R}(s_0)-\boldsymbol{R}(s)\}}{r^2}\Phi(s) + \tfrac{2}{3}\{\boldsymbol{n}_-(s)\cdot\boldsymbol{R}(s)\}\log r_- + \frac{\boldsymbol{n}_-(s)\cdot\{\boldsymbol{R}(s_0)-\boldsymbol{R}_-(s)\}}{r_-^2}\Phi(s)\right]\mathrm{d}s, \tag{62}$$

where $\boldsymbol{R}_-(s) = (X(s), -Y(s))$, $r_- = |\boldsymbol{R}_-(s) - \boldsymbol{R}(s_0)|$ and $\boldsymbol{n}_-(s) = (-Y'(s), -X'(s))$.

We truncate the free surface at $s = s_N$ and represent it using N points, not necessarily equally spaced, at which $s = s_i \geqslant 0$ for $i = 1, 2, \ldots, N$, with $s_1 = 0$. This divides the surface into $N-1$ elements, each with arclength $\Delta s_i = s_{i+1} - s_i$. At these points, we define the $3N$ unknowns $X_i = X(s_i)$, $Y_i = Y(s_i)$ and $\Phi_i = \Phi(s_i)$.

We evaluate (18) at the midpoint of each element, $s = s_i + \frac{1}{2}\Delta s_i$ for $i = 1, 2, \ldots, N-1$, approximating the first derivatives using central differences. We evaluate (19) at the points $s = s_i$ for $i = 1, 2, \ldots, N-1$, using a four-point formula to evaluate the first derivatives, and a central three-point formula to evaluate the second derivatives. We found that using a three-point formula for the first derivative (central differences on a uniformly spaced grid), leads to grid-scale oscillations in Φ.

We solve the boundary integral equation, (62), by collocating at the midpoint of each element; in other words, we choose $s_0 = s_i + \frac{1}{2}\Delta s_i$ for $i = 1, 2, \ldots N-1$. When solving (62), we assume that X, Y and Φ vary linearly along each element. This allows us to evaluate the integral on each element analytically. The advantages of this approach are firstly that we do not need to worry about the logarithmic singularity in the integrand, and secondly that, when the free surface approaches the x-axis and becomes close to its image in the x-axis, we maintain accuracy as r_- in (62) becomes small. This provides us with $3N-3$ equations. The remaining three equations are provided by the boundary conditions,

$$Y_1 = 0, \quad Y_N\cos\alpha = X_N\sin\alpha, \quad \Phi_N = 0. \tag{63}$$

Recall that $\epsilon = \tan\alpha$. Note that we do not need to impose the symmetry conditions $X'(0) = \Phi'(0) = 0$, since these are implicit in (62).

We solve the system of $3N$ nonlinear algebraic equations provided by this discretization using Newton's method and continuation. We start with α close to 90°,

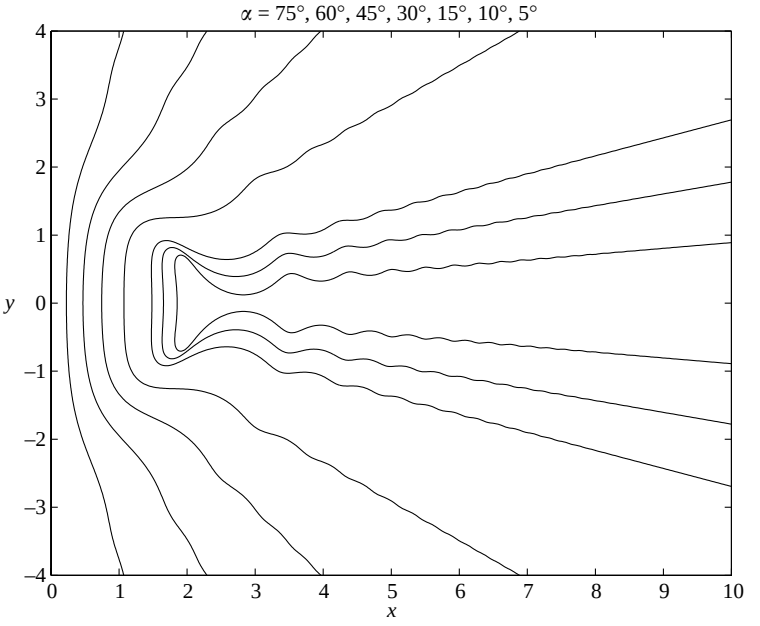

FIGURE 2. The solution for various $\alpha \geqslant 5^\circ$.

with $X_i = \Phi_i = 0$ and $Y_i = s_i$, the solution when $\alpha = 90^\circ$, as the initial guess. We then decrease α and use the solution calculated previously as our initial guess. The major bottleneck in this method is the calculation of the Jacobian, which we perform using finite differences. We therefore reuse the Jacobian at each step of the Newton iteration, and for successive values of α, until progress slows to an unacceptable rate, when we recalculate the Jacobian using the current solution.

Figure 2 shows the shape of the free surface for various values of $\alpha \geqslant 5^\circ$. Figure 3 shows the shape of the free surface for smaller values of α. In each case, we used a uniform grid, with $s_N = 12$ and $N = 600$. Tests with different values of N and s_N confirmed that these solutions have converged. We can see that, as α decreases, capillary waves of increasing amplitude form on the free surface. The amplitude of these waves becomes large enough that, at a finite value of $\alpha = \alpha_0 \approx 2.87^\circ$, the free surface touches itself on the axis of symmetry. This result was first reported by Keller, Milewski & Vanden-Broeck (2000). It is now clear why we were unable to find a solution of the nonlinear integral equation (60), which represents the inner solution in the limit $\alpha \to 0$, since the solution only exists for a finite range of values of $\alpha > \alpha_0$.

2.3. *The effect of a low-density interior fluid*

The results of the previous section suggest that, for $\alpha \leqslant \alpha_0$, the free surface may not be simply connected. When there is no fluid inside the slender wedge ($\rho \equiv \rho_2/\rho_1 = 0$) there is nothing to rule out this situation. In contrast, if there is a fluid inside the wedge, however small its density, the free surface must be simply connected. If a disconnected region of the interior fluid existed, since lengths scale with $t^{2/3}$, its area would grow like $t^{4/3}$. Since there are no sources of the fluid, this is not possible. This means that the limit $\rho \ll 1$ is a singular perturbation, since solutions with $\rho = 0$ may be qualitatively different from solutions with $0 < \rho \ll 1$. This leads us to consider what happens to the solution when a low-density fluid exists inside the slender wedge; the double limit, $\epsilon \ll 1$, $\rho \ll 1$.

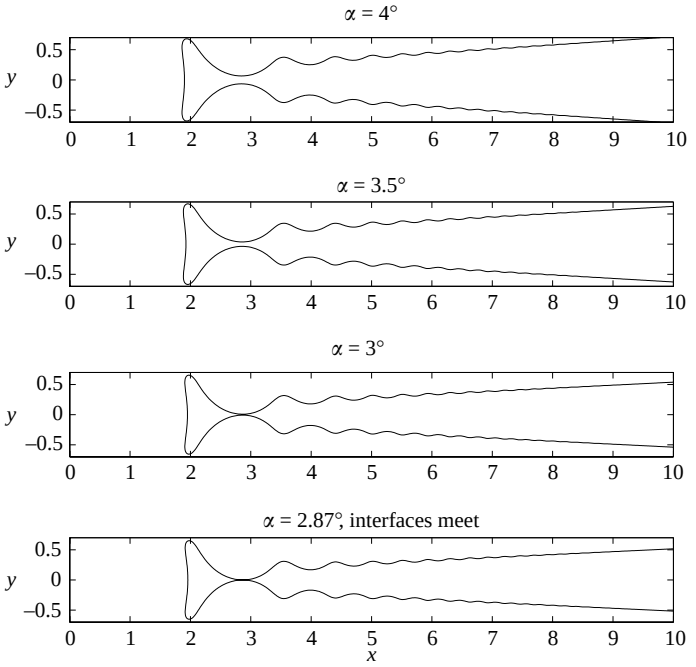

FIGURE 3. The solution for various $\alpha \leqslant 4^\circ$.

The outer solution described in § 2.1.1 is unaffected by the inclusion of an interior fluid of low density. It is straightforward to solve for the flow of the low-density fluid, which is one-dimensional at leading order, but we will not give the details here.

As we shall see below, the inner solution described in § 2.1.2 is affected. An appropriate scaling for the potential inside the wedge, ϕ_2 is

$$\phi_2 = \epsilon^{-4/9} c + \tfrac{2}{3}\epsilon^{2/9} \bar{X}_0^{-1} \hat{x} + \epsilon^{8/9} \bar{X}_0^{-1} \hat{\phi}_2, \tag{64}$$

where c is a constant. The first two terms of this expression come from matching with the outer solution. At leading order, we find that

$$\nabla^2 \hat{\phi}_2 = 0 \quad \text{in } D_2, \tag{65}$$

subject to

$$\hat{\Phi}_{2n} \equiv -\hat{Y}' \frac{\partial \hat{\phi}_2}{\partial \hat{x}} + \hat{X}' \frac{\partial \hat{\phi}_2}{\partial \hat{y}} = \tfrac{2}{3} \bar{X}_0^{-3} (-\hat{Y}' \hat{X} + \hat{X}' \hat{Y}) = \tfrac{2}{3} \bar{X}_0^{-3} \hat{\boldsymbol{n}} \cdot \hat{\boldsymbol{R}} \quad \text{on } \partial D. \tag{66}$$

These are the governing equations for potential flow in D_2 with a flux through the boundary given by (66). The position of the boundary, and hence this flux, is determined by the solution of the problem for $\hat{\phi}_1$, which is slightly different to that discussed in § 2.1.2. The Bernoulli condition, (47), becomes

$$\tfrac{1}{2}(\hat{\Phi}_1')^2 - \tfrac{2}{9} - \tfrac{1}{2}\rho\epsilon^{4/3}(\hat{\Phi}_2')^2 + O(\rho) = -\hat{Y}''\hat{X}' + \hat{X}''\hat{Y}'. \tag{67}$$

We have retained just one additional term relating to the flow inside the wedge, which we shall see becomes important in an inner-inner region.

Let us now assume that a narrow neck, with width δ, forms at $\hat{x} = \hat{X}_1$ in the interior fluid as $\epsilon \to 0$, as sketched in figure 4. This neck divides D_2 into the areas D_- and D_+. On the line L_0, which crosses the neck, $\partial\hat{\phi}_2/\partial n \approx \delta \hat{\Phi}_2'$, whilst on the rest of the

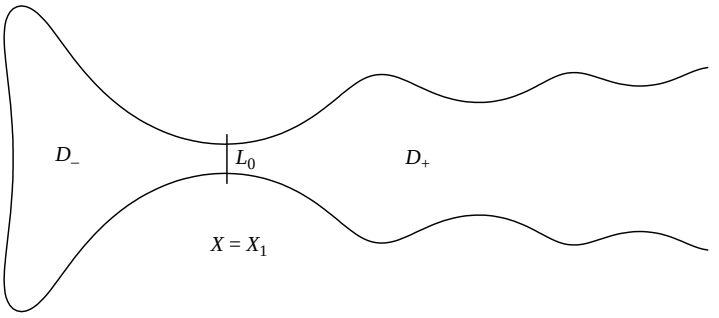

FIGURE 4. The neck in D_2, the regions $D_\pm$ and the line L_0.

boundary of D_-, $\partial\hat{\phi}_2/\partial n$ is given by (66). This means that $\hat{\Phi}_2' = O(\delta^{-1})$ for $\delta \ll 1$. We therefore expect that when $\delta = O(\rho^{1/2}\epsilon^{2/3})$, the flow of the interior fluid will start to affect the shape of the free surface, as determined by the inner solution, through (67). This is just the Bernoulli effect, which operates when the neck is narrow enough that the flow of the light interior fluid is sufficiently rapid that it significantly affects the pressure there, and hence the shape of the free surface. However, we will concentrate on what happens when $\delta = O(\rho\epsilon^{4/3})$, and the flow of the interior fluid dominates the behaviour of the free surface at the neck, since we can then solve for the flow in the neck without solving the inner problem.

2.3.1. *Inner-inner, or neck, problem*

We define the inner-inner variables to be

$$\left.\begin{aligned} \hat{x} &= \hat{X}_1 + \rho\epsilon^{4/3}\bar{\hat{x}}, \quad \hat{y} = \rho\epsilon^{4/3}\bar{\hat{y}}, \quad \hat{s} = \rho\epsilon^{4/3}\bar{\hat{s}}, \\ \hat{X} &= \hat{X}_1 + \rho\epsilon^{4/3}\bar{\hat{X}}, \quad \hat{Y} = \rho\epsilon^{4/3}\bar{\hat{Y}}, \quad \hat{\phi}_2 = \bar{\hat{\phi}}. \end{aligned}\right\} \tag{68}$$

At leading order in terms of these new variables, we obtain

$$\nabla^2\bar{\hat{\phi}} = 0 \quad \text{for } \bar{\hat{y}} < \bar{\hat{Y}}, \tag{69}$$

subject to

$$\frac{\partial\bar{\hat{\phi}}}{\partial n} = 0 \quad \text{on } \bar{\hat{y}} = \bar{\hat{Y}}, \tag{70}$$

$$\frac{\partial\bar{\hat{\phi}}}{\partial\bar{\hat{y}}} = 0 \quad \text{on } \bar{\hat{y}} = 0, \tag{71}$$

$$\bar{\hat{\kappa}} = -\tfrac{1}{2}(\bar{\hat{\Phi}}')^2 \quad \text{on } \bar{\hat{y}} = \bar{\hat{Y}}. \tag{72}$$

In order to obtain the matching conditions with the inner problem, we note that the inner flow will see the neck region as a point, and therefore that the flow out of D_- must exit through a point source at the neck. We can obtain the total flow out of D_- by integrating (67) over the boundary, which gives a value of $-\frac{4}{3}\bar{X}_0^{-3}\bar{D}_-$, where $\bar{D}_-$ is the area of D_-. In other words, the flow is actually directed into D_- through the neck. If we assume that

$$\bar{\hat{Y}} \sim -\tan\beta\,\bar{\hat{X}} \quad \text{as } \bar{\hat{X}} \to -\infty, \tag{73}$$

$$\bar{\hat{Y}} \sim \tan\gamma\,\bar{\hat{X}} \quad \text{as } \bar{\hat{X}} \to \infty, \tag{74}$$

we deduce that

$$\bar{\hat{\phi}} \sim \frac{K}{\beta} \log \bar{\hat{r}} \quad \text{as } \hat{r} \to \infty \text{ with } \tfrac{1}{2}\pi - \beta \leqslant \theta \leqslant \tfrac{1}{2}\pi, \tag{75}$$

$$\bar{\hat{\phi}} \sim -\frac{K}{\gamma} \log \bar{\hat{r}} \quad \text{as } \hat{r} \to \infty \text{ with } 0 \leqslant \theta \leqslant \gamma, \tag{76}$$

where $(\bar{\hat{r}}, \theta)$ are polar coordinates and $K = \frac{2}{3}\bar{X}_0^{-3}\bar{D}_-$.

We can now solve this problem using the complex variable method described in § 2.1.2. For this problem, we find that $\tau \equiv \log q$ satisfies

$$\tau_{\phi\phi} + \tau_{\psi\psi} = 0 \quad \text{for } 0 < \psi < K, -\infty < \phi < \infty, \tag{77}$$

subject to

$$\tau_\psi = \begin{cases} 0 & \text{on } \psi = K \quad \text{for } -\infty < \phi < \infty, \\ \frac{1}{2}\mathrm{e}^\tau & \text{on } \psi = 0 \quad \text{for } -\infty < \phi < \infty, \end{cases} \tag{78}$$

$$\tau \sim \begin{cases} -\dfrac{\beta}{K}\phi + \log\left(\dfrac{K}{\beta}\right) & \text{as } \phi \to \infty, \\ \dfrac{\gamma}{K}\phi + \log\left(\dfrac{K}{\gamma}\right) & \text{as } \phi \to -\infty. \end{cases} \tag{79}$$

We can conformally map this problem in a strip onto an upper half-plane using $W = \mathrm{e}^{\pi w/K}$. After also making the definition

$$\tau = -\frac{\beta}{\pi} \log r + \log\left(\frac{K}{\beta}\right) + \bar{\tau},$$

we obtain

$$\bar{\tau}_{\Phi\Phi} + \bar{\tau}_{\Psi\Psi} = 0 \quad \text{for } \Psi > 0, -\infty < \Phi < \infty, \tag{80}$$

subject to

$$\hat{\tau}_\Psi = \begin{cases} 0 & \text{on } \Psi = 0 \text{ for } \Phi < 0, \\ -\dfrac{K^2}{2\pi\beta}\Phi^{-(1+\beta/\pi)}\mathrm{e}^{\bar{\tau}} & \text{on } \Psi = 0 \text{ for } \Phi > 0, \end{cases} \tag{81}$$

$$\bar{\tau} \to 0 \quad \text{as } \Phi^2 + \Psi^2 \to \infty, \tag{82}$$

where $W = \Phi + \mathrm{i}\Psi$. We are also left with a singularity at the origin, with

$$\bar{\tau} \sim \frac{\gamma + \beta}{\pi} \log|\Phi| + \log\left(\frac{\beta}{\gamma}\right) \quad \text{as } \Phi \to 0 \text{ on } \Psi = 0. \tag{83}$$

We can reformulate this as the single integral equation

$$\bar{\tau}(\Phi, 0) = \frac{\gamma + \beta}{\pi} \log|\Phi| - \frac{K^2}{2\pi^2\beta} \int_0^\infty \xi^{-(1+\beta/\pi)} \exp\{\bar{\tau}(\xi, 0)\} \log|\xi - \Phi| \, \mathrm{d}\xi, \tag{84}$$

but note that we must still satisfy (83), since this tells us two terms in the local expansion of $\bar{\tau}$. We also note that the solvability condition for the Neumann boundary value problem is

$$\frac{\gamma + \beta}{\pi} = \frac{K^2}{2\pi^2\beta} \int_0^\infty \xi^{-(1+\beta/\pi)} \exp\{\bar{\tau}(\xi, 0)\} \, \mathrm{d}\xi, \tag{85}$$

and that, after taking the small-Φ limit of (84), (83) shows that

$$\log\left(\frac{\beta}{\gamma}\right) = -\frac{K^2}{2\pi^2\beta}\int_0^\infty \xi^{-(1+\beta/\pi)}\exp\{\bar{\tau}(\xi,0)\}\log\xi\,\mathrm{d}\xi. \tag{86}$$

In order to rewrite (83) and (84) in a form more suitable for numerical solution, we define

$$\Phi = \left(\frac{K^2}{2\pi^2\beta}\right)^{\pi/\beta}\bar{\Phi}, \quad \xi = \left(\frac{K^2}{2\pi^2\beta}\right)^{\pi/\beta}\bar{\xi},$$

which, after making use of the solvability condition, eliminates K from the integral equation, giving

$$\bar{\tau}(\bar{\Phi},0) = \frac{\gamma+\beta}{\pi}\log|\bar{\Phi}| - \int_0^\infty \bar{\xi}^{-(1+\beta/\pi)}\exp\{\bar{\tau}(\bar{\xi},0)\}\log|\bar{\xi}-\bar{\Phi}|\,\mathrm{d}\bar{\xi}. \tag{87}$$

Similarly, (85) and (86) become

$$\frac{\gamma+\beta}{\pi} = \int_0^\infty \bar{\xi}^{-(1+\beta/\pi)}\exp\{\bar{\tau}(\bar{\xi},0)\}\,\mathrm{d}\bar{\xi}, \tag{88}$$

$$\log\left(\frac{\beta}{\gamma}\right) + \frac{\gamma+\beta}{\beta}\log\left(\frac{K^2}{2\pi^2\beta}\right) = -\int_0^\infty \bar{\xi}^{-(1+\beta/\pi)}\exp\{\bar{\tau}(\bar{\xi},0)\}\log\bar{\xi}\,\mathrm{d}\bar{\xi}. \tag{89}$$

Finally, we subtract $\log|\bar{\Phi}|$ times (88) from (87) to obtain

$$\bar{\tau}(\bar{\Phi},0) = -\int_0^\infty \bar{\xi}^{-(1+\beta/\pi)}\exp\{\bar{\tau}(\bar{\xi},0)\}\log\left|1-\frac{\bar{\xi}}{\bar{\Phi}}\right|\mathrm{d}\bar{\xi}. \tag{90}$$

For a given value of β, we solve (90) numerically, evaluating the integral using the trapezium rule, after subtracting out the integrable singularities at $\bar{\xi}=0$ and $\bar{\xi}=\bar{\Phi}$. Knowing $\bar{\tau}$, we can then obtain the corresponding value of γ from (88) and K from (89). In this way, we can determine how β and γ vary with K, which is half the flux through the neck.

For $\bar{\Phi}\gg 1$, $\bar{\tau} = O(\bar{\Phi}^{-\beta/\pi})$. This means that we need a very long range of integration to be able to capture the behaviour of $\bar{\tau}$, particularly when β is small. In order to accommodate this, we discretized $\bar{\tau}$ on a logarithmically spaced grid of 3000 points, truncating the domain at a value of $\bar{\xi}=\bar{\xi}_N$ large enough that $\bar{\tau}(\bar{\xi}_N) < 10^{-8}$. Figure 5 shows the solution when $\beta=\pi/4$, which we can see is in good agreement with the known large- and small-$\bar{\xi}$ behaviour, although we note that $\bar{\tau}$ deviates from the expected behaviour close to the end of the truncated domain, where it is very small. As we might expect from the symmetry of the problem, we find that $\beta=\gamma$ to numerical accuracy, and that these angles vary with K in the manner shown in figure 6. The larger K, the larger the flux through the neck, and the larger the angles β and γ.

2.3.2. *Inner problem*

On the inner length scale, the neck, or inner-inner, region is a point. We must therefore solve the same boundary value problem that we obtained at leading order when $\rho=0$, (45) to (52), but now with the added condition that the free surface touches the $\hat{x}$-axis at some point $\hat{x}=\hat{X}_1$. The neck solution also shows that the free surface makes the same angle, $\beta(K)$, with the $\hat{x}$-axis on either side of this point. We can still reformulate the problem in terms of the complex velocity, as we did in § 2.1.2, but now we have another stagnation point on the $\hat{x}$-axis. This means that (60)

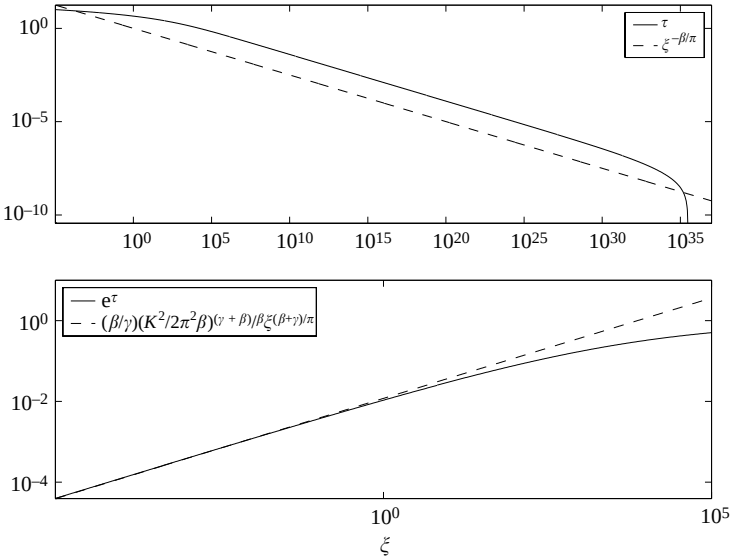

FIGURE 5. The behaviour of $\bar{\tau}$ as $\bar{\xi} \to 0$ and $\bar{\xi} \to \infty$ for a typical case, $\beta = \pi/4$.

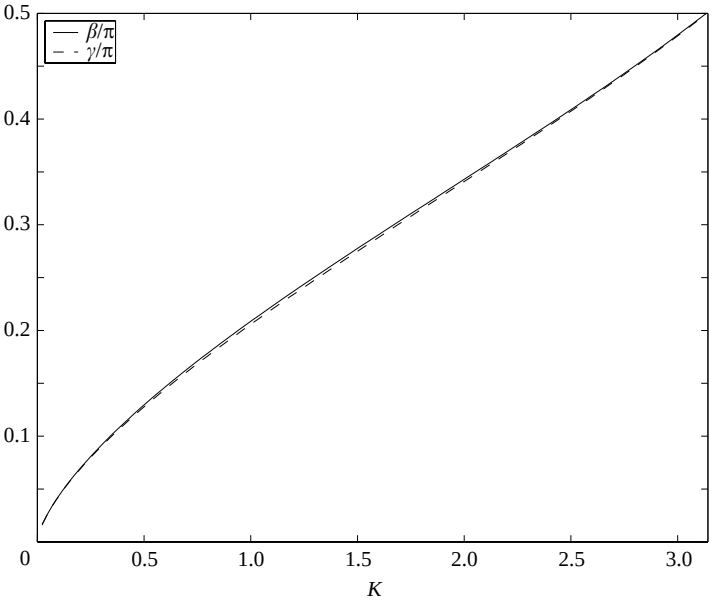

FIGURE 6. The behaviour of $\beta(K)$ and $\gamma(K)$.

becomes

$$\hat{\tau}(\phi, 0) = \frac{1}{2}\log|\phi| + \frac{2\beta}{\pi}\log|\phi - \phi_1| - \frac{2}{3\pi}\int_{-\infty}^{0} \sinh\hat{\tau}(\xi, 0)\log|\xi - \phi|\,\mathrm{d}\xi, \tag{91}$$

where ϕ_1 is the unknown potential at the neck. The condition that the free surface touches the $\hat{x}$-axis is

$$\int_0^{\phi_1} \exp\{-\hat{\tau}(\xi, 0)\}\cos\left\{\int_0^{\xi} \tfrac{2}{3}\sinh\hat{\tau}(\phi', 0)\,d\phi'\right\}\mathrm{d}\xi = 0. \tag{92}$$

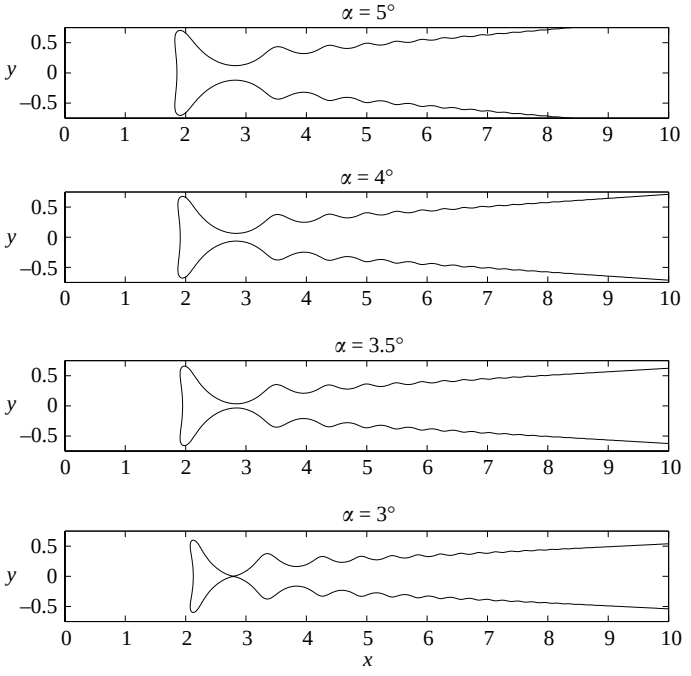

FIGURE 7. The solution for various $\alpha \leqslant 5^\circ$ with $\rho = 0.01$.

The condition that the free surface touches the $\hat{x}$-axis symmetrically is

$$\int_0^{\phi_1} \tfrac{2}{3} \sinh \hat{\tau}(\xi, 0)\, \mathrm{d}\xi = \tfrac{1}{2}\pi + \beta. \tag{93}$$

We can now attempt to solve (91) as we did before, using the trapezium rule, taking into account the integrable singularities of the integrand. Equations (92) and (93) can be treated in the same manner. In principle, we need to solve (91), with the eigenvalues ϕ_1 and β determined by the conditions (92) and (93). If we recall that $K = \frac{2}{3}\bar{X}_0^{-3}\bar{D}_-$, once we have a solution we can calculate the area of D_-, $\bar{D}_-$, and also the value of K that corresponds to $\beta(K)$, and hence determine $\bar{X}_0$. However, even with this modification to the problem, we have been unable to find a solution, although we do not have a proof that no solution exists.

Physically, it is clear why adding the Bernoulli effect has not enabled us to find a solution. The pressure induced by the rapid flow of the interior, low-density fluid through the narrow neck region exerts a force on the exterior fluid directed towards the neck; a suction force. This should cause the free surface to pinch off at larger wedge angles than if the interior fluid were absent. We will now investigate this further by considering the numerical solution of the two-fluid problem.

2.3.3. *Numerical solution*

In order to solve the two-fluid boundary value problem, (11) to (16), we can, as for the single-fluid problem described in § 2.2, use the boundary integral method. The boundary integral equation satisfied by $\Phi_2(s)$, the boundary value of ϕ_2, is also given by (62), but with the direction of $\boldsymbol{n}$ reversed. We discretize Φ_2 at the midpoint of each element, and calculate Φ_2' using central differences. Otherwise, the solution proceeds as before. When $\rho = 0.01$, the results corresponding to those shown in figure 2 are almost identical, since a well-defined neck region has yet to form. Figure 7 shows

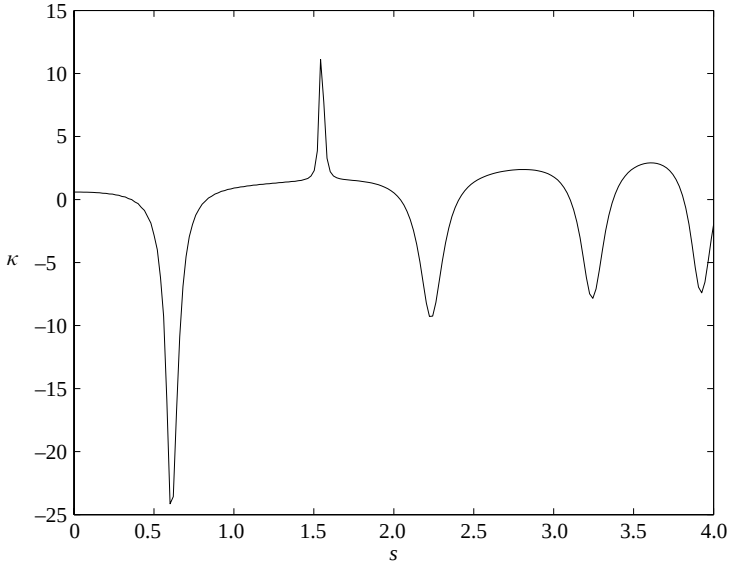

FIGURE 8. The curvature of the free surface when $\alpha = 3^\circ$ and $\rho = 0.01$.

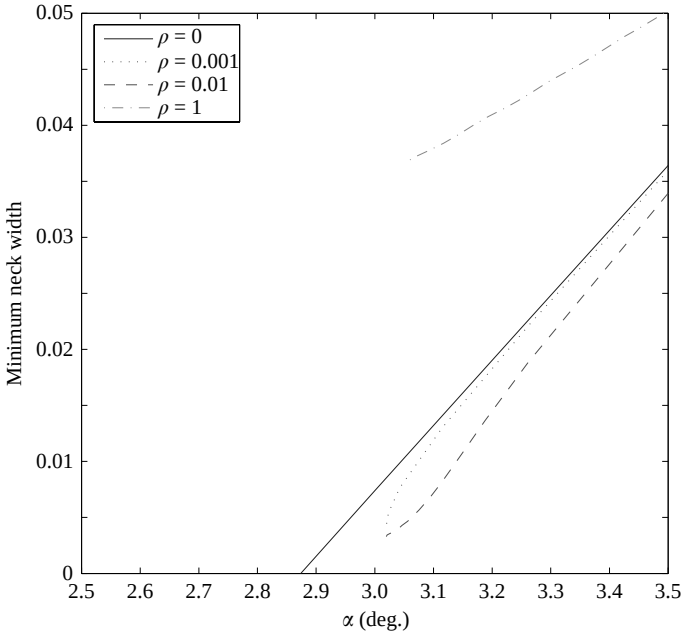

FIGURE 9. The minimum width of the neck for various values of the density ratio, ρ.

the solution as α decreases towards the angle at which the free surface meets the x-axis. Of course, we cannot compute all the way up to the touching angle as we could for the case $\rho = 0$, since Φ_2' becomes unbounded at this angle. We were unable to compute beyond $\alpha = \alpha_0 \approx 3.00^\circ$, at which point the curvature of the free surface, shown in figure 8, is large and rises rapidly at the neck, $s \approx 1.5$, as we would expect.

It is also of interest to investigate how α_0, the minimum value of α for which a similarity solution exists, varies with the density ratio, ρ. Figure 9 shows how the

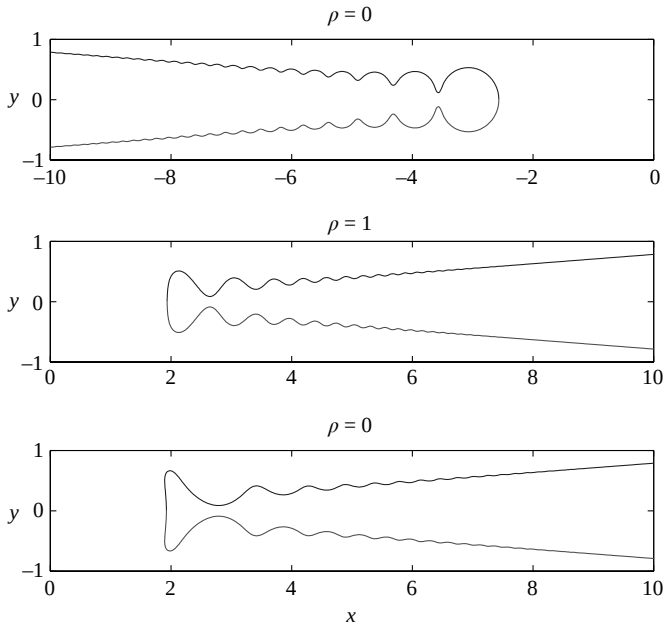

FIGURE 10. The solution for various values of ρ with $\alpha = 4.5°$.

minimum width of the neck varies for several values of ρ. We are not currently able to obtain an accurate solution as α approaches α_0, since the high curvature at the neck is poorly resolved. However, figure 9 suggests that when $\rho < \rho_0$ there is only a solution for $\alpha > \alpha_0(\rho)$, whilst for $\rho > \rho_0$, there is a similarity solution for all $\alpha > 0$. It is, however, rather difficult to determine the values of ρ_0 and $\alpha_0(\rho)$ using our current numerical method. We plan to resolve this issue in the future using an adaptive numerical method, but this is beyond the scope of the present paper. Figure 10 shows how the qualitative form of the solution varies with ρ with α fixed at 4.5°. Note that it is convenient to compute solutions with α close to 180° and $\rho = 0$ to illustrate the solution when the inner fluid is denser than the outer fluid. We are currently investigating the form of the asymptotic solution when $\rho = O(1)$ and $\alpha \ll 1$.

Within the framework of inviscid flow, we conclude that the free surface touches itself on the x-axis at some small finite value of α. If we were to reintroduce the effect of viscosity in the interior fluid at the neck, it is likely that we would be able to construct a solution where the free surface does not touch the x-axis for any $\alpha > 0$, since it takes an infinite time for a viscous lubrication film to thin to zero. However, this type of solution would only be available as an asymptotic solution for $t \gg 1$. In addition, the asymptotic scalings would depend explicitly on t, not just through the similarity variables (9). Moreover, it is likely that lateral instabilities would cause the thin film to rupture at some point. We prefer to continue to investigate this problem for purely inviscid flow.

3. Unsteady solutions

Having now established that, below some critical initial wedge semi-angle, $\alpha = \alpha_0$, for sufficiently small density ratio ρ, the boundary value problem (11) to (16) has no solution, we need to take a step back and consider the original initial value problem,

(1) to (8). Although we have ruled out the idea of including the effect of viscosity in the thin film at the neck, it seems that we need to invoke viscosity at small times. It can be shown that the small-time solution of the equivalent initial value problem when viscosity is included is dominated by viscous forces, and that the free surface is monotonic and simply connected (Billingham 2005). Since the inviscid similarity solution is the natural large-time asymptotic solution of this initial value probem, we hypothesize that, for $\alpha > \alpha_0$, the solution of the viscous initial value problem asymptotes to the inviscid similarity solution as $t \to \infty$, although this may not be uniform in space. This has already been established for $|\alpha - \pi/2| \ll 1$ in Billingham (1999). For $0 < \alpha \leqslant \alpha_0$, we hypothesize that the free surface pinches off for the first time at some finite time t_1. This process then repeats itself, and the free surface pinches off at a sequence of times $t_1, t_2, \ldots$.

Although it is, of course, not unusual to invoke the action of viscosity to regularize an inviscid problem, we believe that this is quite an unusual example. For $\alpha > \alpha_0$, an inviscid similarity solution exists, and is physically reasonable, whilst, for $\alpha \leqslant \alpha_0$, an inviscid similarity solution does not exist. However, on invoking the effect of viscosity to enable the existence of an effective initial condition other than a wedge, we postulate that a physically reasonable inviscid solution again exists, but is unsteady. Moreover, viscosity is not needed to regularize the unsteady solution for $t > 0$; viscosity is only necessary when $t = 0^+$, to blunt the initial wedge.

We will investigate these hypotheses by solving the single-fluid inviscid initial value problem, (1) to (8), but replacing the initial condition (7) with

$$\phi \equiv \phi_1(x, y, 0) = 0 \quad \text{in } D_1 \equiv D, \qquad Y(s, 0) = Y_{\text{in}}(s), \qquad X(s, 0) = X_{\text{in}}(s). \tag{94}$$

The initial position of the free surface, $(X_{\text{in}}(s), Y_{\text{in}}(s))$, must satisfy (6) and (8), and also have the same enclosed area as the original wedge, so that we require

$$\int_0^\infty \{Y_{\text{in}}(s) - \tan\alpha X_{\text{in}}(s)\} X'_{\text{in}}(s)\,\mathrm{d}s = 0. \tag{95}$$

The idea is that this simulates the simply connected free surface shape that emerges from the period when the effect of viscosity is important, and then develops with viscosity negligible as $t \to \infty$.

3.1. *Numerical solution*

In order to solve this problem numerically, it is convenient to make the similarity transformation (9), but retain the time dependence of the variables. In this way, we solve the full, time-dependent inviscid problem, but in a frame of reference that grows like $t^{2/3}$. In this manner, we can keep the solution, which is, of course, always recoiling under the action of surface tension (there is no steady solution in terms of the original, physical variables), within our computational domain. We also define $\tau = \log t$, since this removes any explicit time dependence from the governing equations, and leaves us with an unsteady version of (17) to (23), namely

$$\nabla^2\phi = 0 \quad \text{in } D, \tag{96}$$

$$\frac{\mathrm{d}\Phi}{\mathrm{d}\tau} = Y''X' - X''Y' - \tfrac{1}{3}\Phi + \tfrac{2}{3}\boldsymbol{R}\cdot\nabla\phi - \tfrac{1}{2}|\nabla\phi|^2 + \left(\boldsymbol{n}\cdot\nabla\phi - \tfrac{2}{3}\boldsymbol{n}\cdot\boldsymbol{R}\right)\boldsymbol{n}\cdot\nabla\phi, \tag{97}$$

$$\frac{\mathrm{d}\boldsymbol{R}}{\mathrm{d}\tau} = \left(\boldsymbol{n}\cdot\nabla\phi - \tfrac{2}{3}\boldsymbol{n}\cdot\boldsymbol{R}\right)\boldsymbol{n}, \tag{98}$$

$$\phi_y(x, 0) = 0 \quad \text{for } x < X_0. \tag{99}$$

We discretize the free surface at a set of Lagrangian points $\boldsymbol{R}_i(\tau) = (X_i(\tau), Y_i(\tau))$, at which we also calculate the potential, $\Phi_i(t) = \phi(\boldsymbol{R}_i(t))$. We solve (97) and (98) using the Crank–Nicolson method, calculating $\boldsymbol{n}\cdot\nabla\phi$ at the free surface using the boundary integral equation (62), as described in § 2.2. However, for this unsteady calculation we use cubic splines to calculate the curvature of the free surface and the direction of the normal, $\boldsymbol{n}$. For consistency with the discretization we used for the steady problem, we use 600 points for $0 \leqslant s \leqslant 12$, and then extend the free surface with a further 150 grid points with gradually increasing spacing, up to $s = 1000$. We found that we needed to take this large domain in order to maintain numerical accuracy and stability. After each time step, we regrid the surface using the cubic spline approximation, in order to maintain the initial spacing.

In order to suppress the short-wavelength instability that develops in this, and some other, simulations of invisicid free surface flows, as first noted by Longuet-Higgins & Cokelet (1976), we modify (98) to include a fourth-order diffusive term with small coefficient, which suppresses this instability (see Lundgren & Mansour 1988). We solved

$$\frac{\mathrm{d}\boldsymbol{R}}{\mathrm{d}\tau} = \left(\boldsymbol{n}\cdot\nabla\phi - \tfrac{2}{3}\boldsymbol{n}\cdot\boldsymbol{R}\right)\boldsymbol{n} - \epsilon'\frac{\partial^4\boldsymbol{R}}{\partial s^4}, \tag{100}$$

with $\epsilon' = 10^{-5}$. Numerical experiments confirmed that, prior to the appearance of the instability, the solutions with $\epsilon' = 0$ and $\epsilon' = 10^{-5}$ were indistinguishable.

Before we can compute some solutions, we need to specify the initial conditions, (94). We use a semicircular nose joined to a free surface profile that decays like x^{-2} to the linear far-field behaviour, given by

$$Y_{\mathrm{in}} = \begin{cases} \sqrt{R^2 - (X_{\mathrm{in}} - x_c)^2} & \text{for } x_c - R \leqslant X_{\mathrm{in}} \leqslant x_c, \\ \epsilon X_{\mathrm{in}}\{1 - \exp(-k(X_{\mathrm{in}} - x_c)^2)\} + \dfrac{R}{1 + (X_{\mathrm{in}} - x_c)^2} & \text{for } X_{\mathrm{in}} \geqslant x_c, \end{cases}$$

$$X_{\mathrm{in}} = s. \tag{101}$$

We choose k and l so that the curvature is continuous at $x = x_c$ and the area constraint (95) is satisfied. Figure 11 shows how this initial profile evolves when $\alpha = 4^\circ$, with $x_c = 3.6$, $R = 0.5$, which gives $k \approx 5.65$ and $l \approx 4.85$. As $\tau \to \infty$, the solution asymptotes to the similarity solution, which is steady in terms of these coordinates. This, and other simulations for various wedge semi-angles with $\alpha > \alpha_0$, suggests that the similarity solution is an attractor for the unsteady inviscid problem, provided that the initial conditions satisfy (6), (8) and (95), so that the similarity solution is the large-time solution of the problem that emerges from the initial viscous-dominated flow, and not just for the initial inviscid wedge configuration. In each case, the steady state to which the solution asymptotes is in reasonable agreement with the steady solutions calculated using a slightly different numerical method in § 2.2.

Figures 12 and 13 show how the free surface develops for $\alpha = 1^\circ$, with $x_c = 6.5$, $R = 0.4$, which gives $k \approx 6.08$ and $l \approx 4.85$. We can see that the free surface develops a shape dominated by a large-amplitude capillary wave, which looks very similar to the shapes with α close to α_0 shown in figure 3. However, as predicted, the free surface meets the x-axis at a finite value of τ. In the present paper, we have not tried to perform surgery on the free surface and calculate its subsequent motion. This is a difficult task numerically, as the motion after surgery is initially dominated by the high curvature at the point of pinch-off, which leads to very violent motion. A similar flow was calculated numerically by Duchemin *et al.* (2003), a paper to which

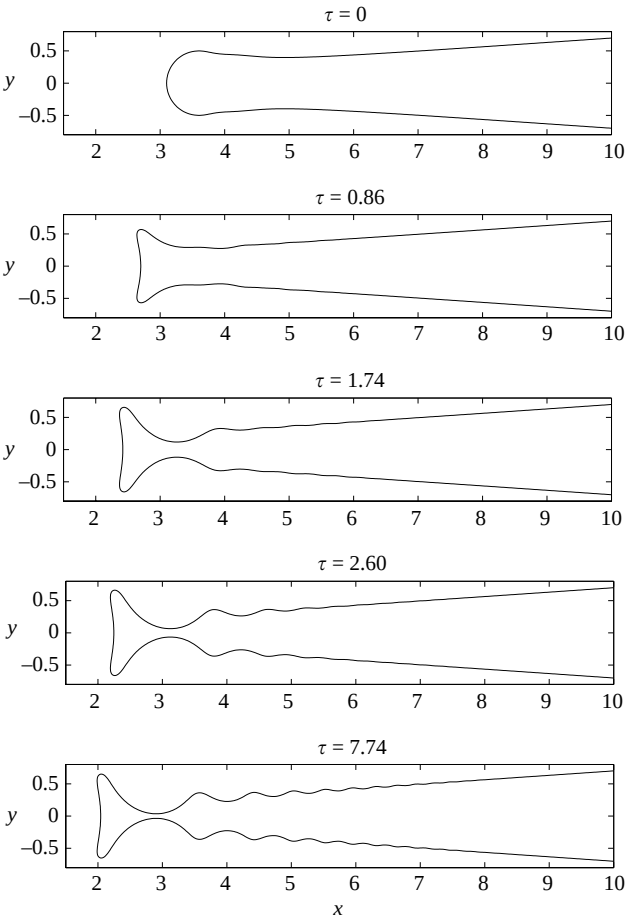

FIGURE 11. The unsteady solution with $\alpha = 4^\circ$ and initial condition given by (101).

we shall return later. These authors were able to proceed past pinch-off by discarding the enclosed bubble and resetting ϕ to zero, effectively starting the fluid from rest.

Figure 14 shows how the free surface develops for $\alpha = 0.1^\circ$, with $x_c = 21.4$, $R = 0.4$, which gives $k \approx 19.91$ and $l \approx 4.98$. Here, although the free surface develops a large-amplitude capillary wave, pinch-off occurs further from the tip than in the previous case. The point of pinch-off is clearly rather sensitive to the precise form of the initial conditions. We will not pursue this further, since the initial conditions that we have used are simply plausible guesses.

We now need to draw a distinction between the cases $\rho = 0$ and $0 < \rho \ll 1$. Firstly, we consider the behaviour close to pinch-off. We have seen above that the interfaces meet in a cusp when $\rho = 0$. When $0 < \rho \ll 1$, for which we have not computed an unsteady solution, we would expect, as discussed in § 2.3, that the rapid flow of the interior low-density fluid through the neck region would suck the free surface together, leading to an outer region where the free surface appears to meet the x-axis at some finite angle β. In fact, the analysis that we gave in § 2.3.1 for the inner-inner, or neck, region remains valid as pinch-off approaches in the unsteady problem. The time-derivative term in the Bernoulli equation does not appear at leading order in the neck region, and the relationship between β and K shown in figure 6 remains valid with K

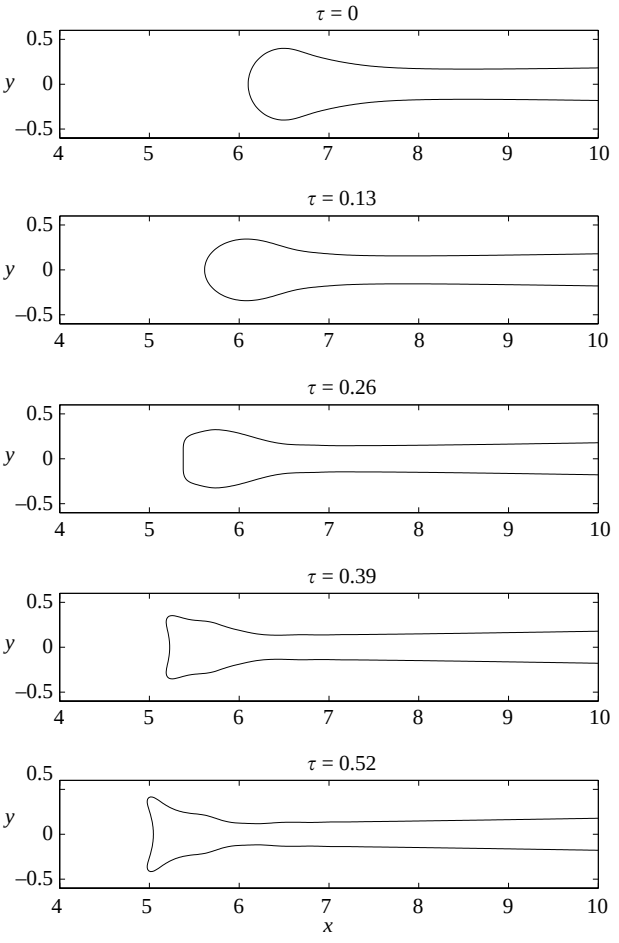

FIGURE 12. The unsteady solution with $\alpha = 1^\circ$ and initial condition given by (101): initial development.

equal to half of the flux through the neck. Secondly, we consider the behaviour after pinch-off. When $\rho = 0$, there is no constraint on the area of the pinched-off bubble, and we cannot say anything about its subsequent behaviour without computing the solution beyond the pinch-off time. However, as we discussed earlier, this is a singular perturbation. When $0 < \rho \ll 1$, there is a fluid within the pinched-off bubble, and its physical area must remain constant. Since we are working in a frame of reference where lengths scale with $t^{2/3}$, the area of the bubble must shrink like $t^{-4/3} = \mathrm{e}^{-4\tau/3}$ in order to remain constant in the original frame of reference. By conservation of mass, as τ increases, the area enclosed by the rest of the free surface must increase and approach its original value. The dynamics of this connected part of the free surface then drives it towards a large-amplitude capillary wave, and pinch-off occurs again. In this way, we can see that the solution is unsteady, with a sequence of pinch-offs and, in this frame of reference, shrinking bubbles.

3.2. *Unsteady asymptotic solution for* $\epsilon \ll 1$

We can now try to construct an asymptotic solution of the unsteady problem valid in the slender wedge limit. We find that we can use the original outer scalings (24).

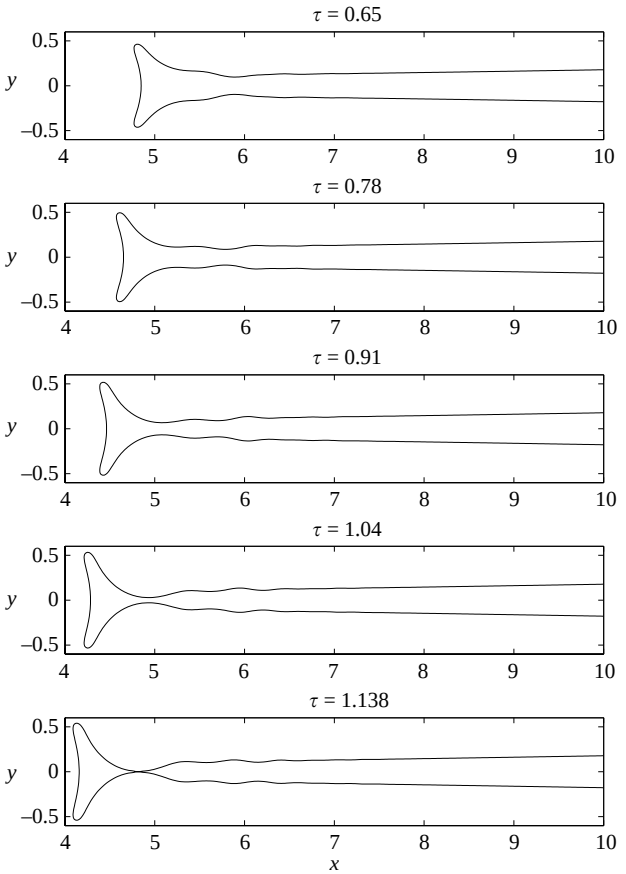

FIGURE 13. The unsteady solution with $\alpha = 1^\circ$ and initial condition given by (101): pinch off.

In the outer region, (27) and (28) become at leading order

$$\frac{\mathrm{d}\bar{\Phi}}{\mathrm{d}\tau} = -\tfrac{1}{3}\bar{\Phi} + \tfrac{2}{3}\bar{x}\bar{\Phi}', \tag{102}$$

$$\frac{\mathrm{d}\bar{Y}}{\mathrm{d}\tau} = \bar{\phi}_{\bar{y}}(\bar{x}, 0) - \tfrac{2}{3}(\bar{Y} - \bar{x}\bar{Y}'). \tag{103}$$

We will not attempt to solve these equations here, although it is possible to do so in principle, but note that now the position of the inner region is time-dependent, with $\bar{X}_0(\tau)$ depending on the matching between the inner and outer regions.

In the inner region, we can use the scalings (45), (47) and (48). However, in order that the time-derivatives appear in the inner equations at leading order, we must define a new, fast time variable, $\hat{\tau} = \epsilon^{-2/3}\bar{X}_0^3(\tau)\tau$, in terms of which, at leading order

$$\nabla^2\hat{\phi} = 0 \quad \text{for } \hat{y} > \hat{Y},\ \hat{x} > 0 \quad \text{and for } \hat{y} > 0,\ \hat{x} < 0, \tag{104}$$

$$\hat{\phi} \sim -\tfrac{2}{3}\hat{x} \quad \text{as } \hat{x}^2 + \hat{y}^2 \to \infty. \tag{105}$$

$$\frac{\mathrm{d}\hat{\Phi}}{\mathrm{d}\hat{\tau}} = -\tfrac{1}{2}|\nabla\hat{\phi}|^2 + \tfrac{2}{9} + \hat{Y}''\hat{X}' - \hat{X}''\hat{Y}', \tag{106}$$

$$\frac{\mathrm{d}\hat{\boldsymbol{R}}}{\mathrm{d}\hat{\tau}} = (\boldsymbol{n}\cdot\nabla\hat{\phi})\boldsymbol{n}, \tag{107}$$

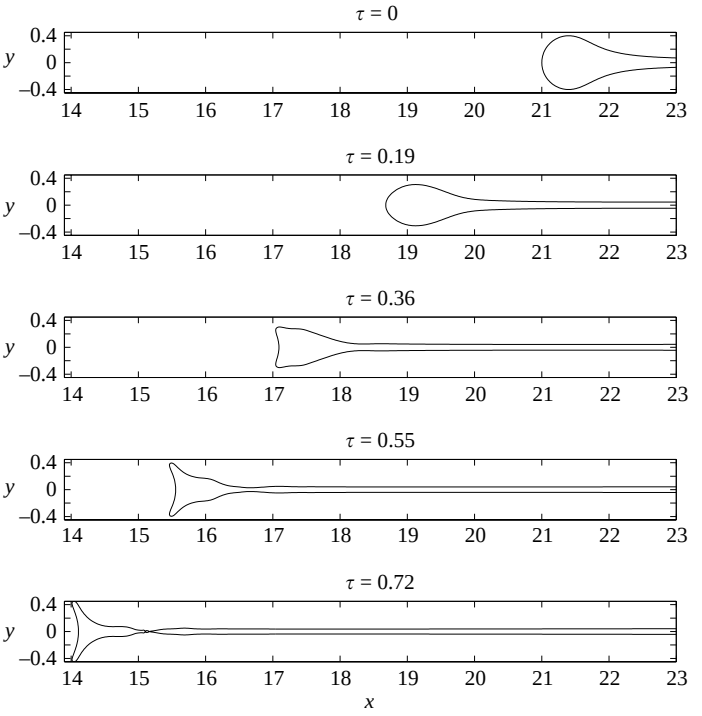

FIGURE 14. The unsteady solution with $\alpha = 0.1^\circ$ and initial condition given by (101).

subject to

$$\hat{\phi} \sim -\tfrac{2}{3}\hat{x} \quad \text{as } \hat{x}^2 + \hat{y}^2 \to \infty. \tag{108}$$

The inner solution develops on this $\tau = O(\epsilon^{2/3})$ timescale, whilst the outer solution, and hence $\bar{X}_0$, develops on a slower, $\tau = O(1)$ timescale, so that $\bar{X}_0$ is constant as far as the inner solution is concerned. After all of the scalings of the original variables, this inner problem is simply the flow of a uniform stream of speed $\frac{2}{3}$ in the negative $\hat{x}$-direction around a region of constant pressure. After subtracting out the flow at infinity, we can solve this problem numerically using the method described in § 3.1.

Before we discuss these solutions, we note that, in this unsteady case, the scalings that we have used for the inner and outer regions are no longer uniquely determined. Since the outer flow develops on a longer timescale than the inner flow, we find that we can reproduce the leading-order inner and outer problems using the more general inner scalings

$$\left.\begin{aligned} &x = \epsilon^{-b/3}\bar{X}_0 + \epsilon^{2b/3}\tilde{X}_0 + \epsilon^{2b/3}\tilde{x}, \quad y = \epsilon^{2b/3}\tilde{y}, \quad X = \epsilon^{-b/3}\bar{X}_0 + \epsilon^{2b/3}\tilde{X}_0 + \epsilon^{2b/3}\tilde{X}, \\ &Y = \epsilon^{2b/3}\tilde{Y}, \quad s = \epsilon^{2b/3}\tilde{s}, \quad \phi = \epsilon^{b/3}\tilde{\phi}, \quad \Phi = \epsilon^{b/3}\tilde{\Phi}, \quad \Phi_n = \epsilon^{-b/3}\tilde{\Phi}_n, \quad \tau = \epsilon^{b}\tilde{\tau}, \end{aligned}\right\} \tag{109}$$

with b a strictly positive constant. The scalings (35) have $b = 2/3$. The outer scalings consistent with this that satisfy $Y - \epsilon X \to 0$ as $s \to \infty$ are

$$\left.\begin{aligned} &x = \epsilon^{-b/3}\bar{x}, \quad y = \epsilon^{-b/3}\bar{y}, \quad X = \epsilon^{-b/3}\bar{X}, \quad Y = \epsilon^{1-b/3}\bar{Y}, \\ &s = \epsilon^{-b/3}\bar{s} \quad \Phi = \epsilon^{1-2b/3}\bar{\Phi}, \quad \Phi_n = \epsilon^{1-b/3}\bar{\Phi}_n. \end{aligned}\right\} \tag{110}$$

Note that, if $\hat{Y} = O(\hat{x}^{-n})$ as $\hat{x} \to \infty$, then matching between the inner and outer regions demands that $\bar{Y} = O((\bar{x} - \bar{X}_0)^{-n})$ as $\bar{x} \to \bar{X}_0$. For this procedure to be consistent, we need

$$n = \frac{1}{b} - 1, \tag{111}$$

a condition that will prove to be important in § 4.

Figure 15 shows the numerical solution of the inner problem with

$$\hat{Y}_{\text{in}} = \begin{cases} \sqrt{R^2 - \hat{X}_{\text{in}}^2} & \text{for } -R \leqslant \hat{X}_{\text{in}} \leqslant 0, \\ \dfrac{R}{1 + l\hat{X}_{\text{in}}^2} & \text{for } \hat{X}_{\text{in}} \geqslant 0, \end{cases} \tag{112}$$

$$\hat{X}_{\text{in}} = s,$$

and $R = 1$ and $l = 1/2/R^2$. We have subtracted out the part of the initial condition (101) that gives linear growth at infinity, and chosen l so that the curvature is continuous at $\hat{x} = 0$. A simple order-of-magnitude estimate shows that the enclosed area in the inner region is of $O(\epsilon^{4b/3})$, whilst the excess area over the original wedge configuration in the outer region is of $O(\epsilon^{1-2b/3})$. Provided $b > \frac{1}{2}$, the area enclosed by the inner region is small relative to the excess area in the outer region, and the initial area can be taken to be arbitrary. This is the case here, where we have taken $b = 2/3$. It is clear from figure 15 that the behaviour of the solution is qualitatively the same as that shown in figure 14, with pinch-off at a finite time in an initially narrow part of the interior fluid.

Figures 16 and 17 show the numerical solution of the inner problem with

$$\hat{Y}_{\text{in}} = \begin{cases} \sqrt{R^2 - \hat{X}_{\text{in}}^2} & \text{for } -R \leqslant \hat{X}_{\text{in}} \leqslant 0, \\ \left\{ R - \left(\dfrac{1}{2R} - R \right) x^2 \right\} e^{-x^2} + \dfrac{x^3}{2(1 + x^{7/2})} & \text{for } \hat{X}_{\text{in}} \geqslant 0, \end{cases} \tag{113}$$

$$\hat{X}_{\text{in}} = s,$$

and $R = 0.5$. This initial condition has an interior region of sufficient width that a large-amplitude capilary wave develops and pinch-off occurs close to the tip. This solution should be compared with figures 12 and 13.

One feature that is obvious from a comparison of the unsteady inner solutions and the full unsteady solutions is that the inner region travels to the left in the full solution. This is because $\bar{X}_0 \equiv \bar{X}_0(\tau)$ in the asymptotic formulation. In other words, $\bar{X}_0$, the position of the inner region relative to the origin, as defined by (35) is fixed by matching with the outer solution, which varies on an $O(1)$ timescale, whilst the flow in the inner region varies on an $O(\epsilon^b)$ timescale.

4. The inviscid coalescence of drops

Duchemin *et al.* (2003, henceforth referred to as DEJ), studied the motion of two spheres or cylinders of fluid, brought together with negligible velocity; a sintering problem. They argued that viscous forces are dominant at very small times, but that the later evolution is essentially inviscid. They showed that the coalescence of spheres is two-dimensional at leading order, and hence equivalent to the coalescence of cylinders. In order to simulate this process, they took two cylinders of inviscid fluid at rest, joined by a very small liquid bridge whose formation was assumed to be under

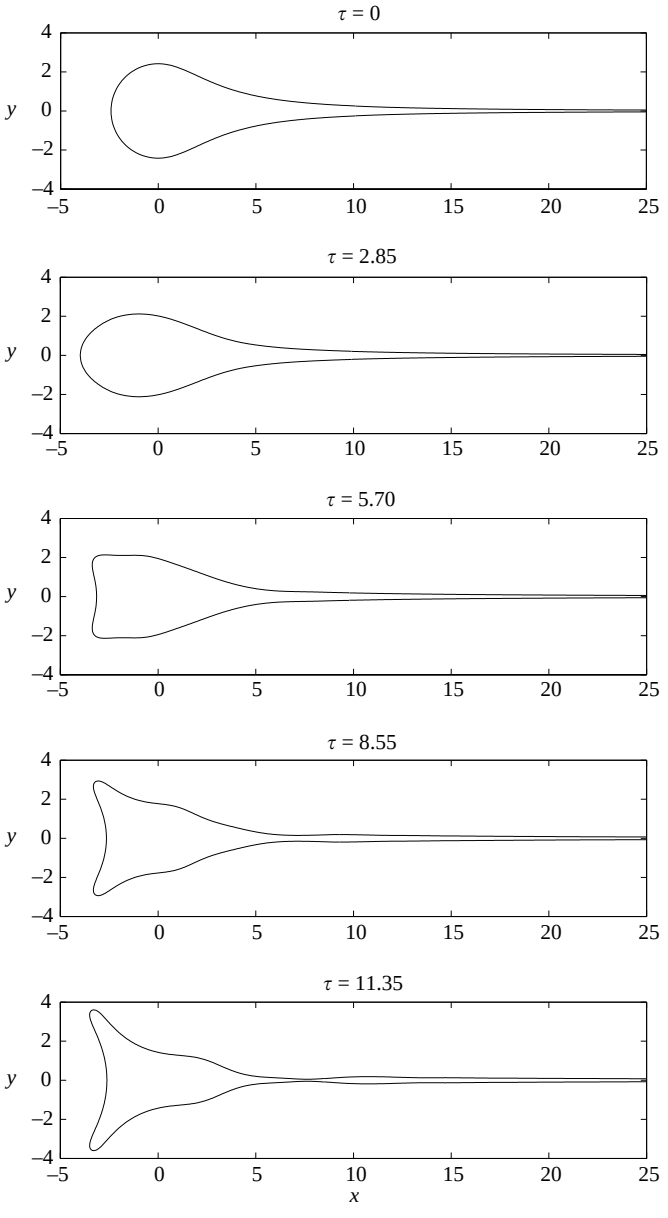

FIGURE 15. The unsteady inner solution with initial condition (112).

the control of first intermolecular, and then viscous forces. Indeed the sintering of two spherical drops by the action of surface diffusion, and at small enough times that viscosity dominates inertia have also been studied (Eggers 1998; Eggers, Lister & Stone 1999). This is basically the same argument that we used in the previous section to justify studying the unsteady problem with non-wedge-shaped initial conditions. DEJ then studied the subsequent inviscid, irrotational motion of the free surface using a boundary integral method. DEJ found, as we have, that there is a succession of pinch-off events during the coalescence process, with the form of the free surface

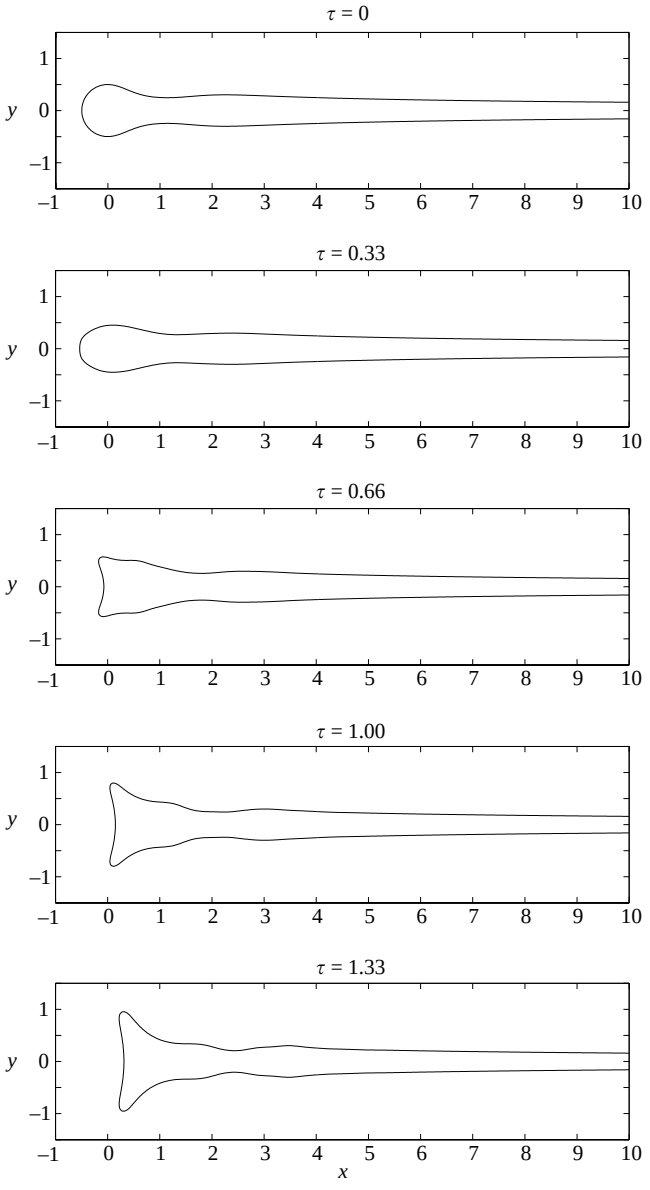

FIGURE 16. The unsteady inner solution with initial condition (113): initial development.

looking strikingly similar to that which we have calculated for the two-dimensional wedge problem.

DEJ use (r, z) coordinates, in terms of which the initial height of the free surface above the r-axis, $w = z$, varies quadratically with r, so that the slope varies linearly with r. In our notation, $\epsilon \sim r$. During any single pinch off in the coalescence problem, r_c, the distance between the initial position of the tip of the free surface, r_b, and the point where the next pinch-off occurs, is small compared to r_b, so that, at leading order, the slope of the free surface, ϵ, is approximately constant. We can therefore apply our slender wedge analysis to this problem. This suggests that $r_c = O(t^{2/3}\epsilon^{2b/3})$, consistent with this assumption, and also that $r_b = O(t^{2/3}\epsilon^{-b/3})$. Since we already have

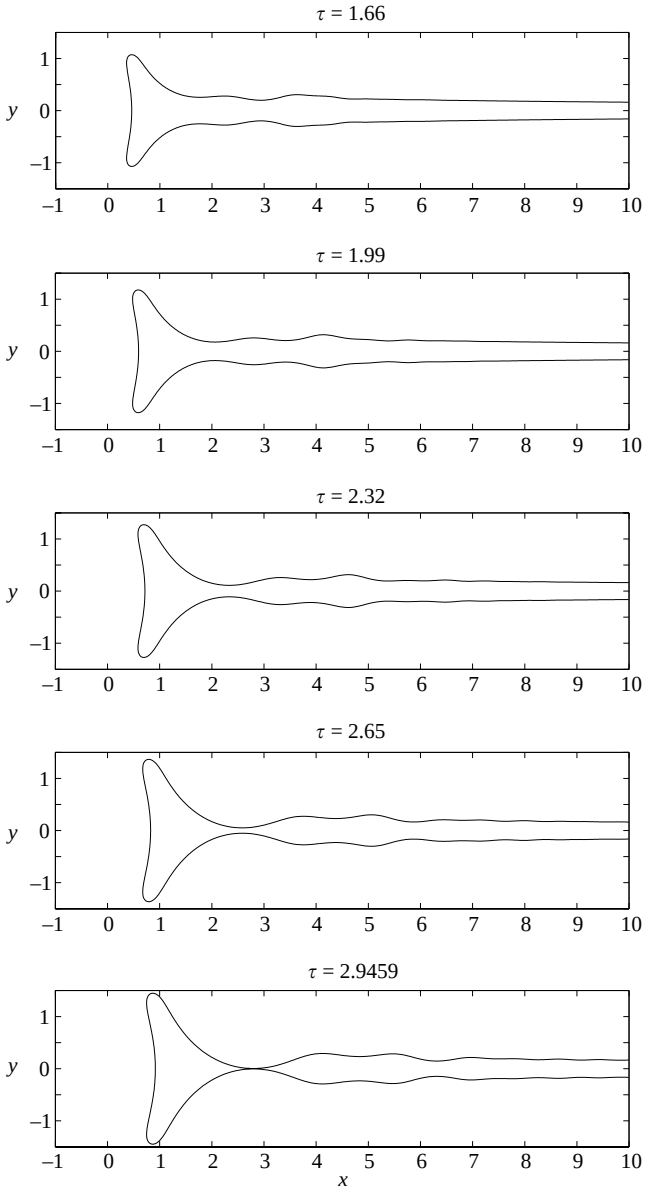

FIGURE 17. The unsteady inner solution with initial condition (113): pinch off.

$r_b = O(\epsilon)$, this immediately gives us

$$r_b = O(\epsilon) = O\left(t^{2/(b+3)}\right), \quad r_c = O\left(t^{2(b+1)/(b+3)}\right). \tag{114}$$

In order to fix b, we note that, in contrast to the slender wedge problem, the tangent to the free surface during a pinch-off event in coalescence, which we treat as if it were a slender wedge, does not pass through the origin. In order to be consistent with this constant offset, we need $\hat{Y}$ to tend to a constant as $\hat{x} \to \infty$, out of the inner region. Equation (111) shows that, in order for this to match to a sensible outer solution, we require $b = 1$. The scalings (114) with $b = 1$ are precisely those found by DEJ.

DEJ also go on to analyse the scaling laws for the time and distance between successive pinch-offs. Equation (114) is consistent with their estimate of r_c, the distance between pinch-offs. Fron our analysis, the time between pinch-offs is

$$\tau_{n+1} - \tau_n = O(\epsilon^b),$$

and hence

$$t_{n+1} - t_n = O(\epsilon^b t_n) = O\left(t^{3(b+1)/(b+3)}\right), \tag{115}$$

which, again, reproduces DEJ's result when $b = 1$. Finally, we have found that pinch-off occurs for $\alpha < \alpha_0 \approx 2.87^\circ$, which is equivalent to $\epsilon \leqslant \epsilon_0 \approx 0.05$. This is precisely the estimate given by DEJ.

We can also make this argument more formal. If we assume that the initial shape of the free surface away from the rounded tip is $Y = x^2/2R_b$, where R_b is the radius of the cylinders, we can use dimensionless variables

$$r = \frac{x}{R_b}, \quad z = \frac{y}{R_b}, \quad w = \frac{Y}{R_b}, \quad T = \frac{\sigma^{1/2} t}{\rho^{1/2} R_b^{3/2}}, \tag{116}$$

in terms of which the far field becomes $w = \frac{1}{2}r^2$. Our earlier arguments show that we need to look for an inner solution using

$$T = \epsilon^{(b+3)/2}\bar{T}, \quad r = \bar{T}^{2/3}(\epsilon \bar{R}_0 + \epsilon^{b+1}\tilde{r}), \quad w = \bar{T}^{2/3}\epsilon^{b+1}\tilde{w}, \quad \tau = \log T = \epsilon^b \bar{\tau}. \tag{117}$$

In terms of these variables, the matching condition provided by the shape of the free surface far from the tip is

$$\tilde{w} \sim \tfrac{1}{2}\bar{T}^{2/3}\epsilon^{1-b}\bar{R}_0^2 \quad \text{as } \tilde{r} \to \infty. \tag{118}$$

As we would expect in this problem, where there is a lengthscale, R_b, this remains dependent upon time, $\bar{T}$. However, the key point is that, during a pinch-off event, $\bar{T}$ only changes by an $O(\epsilon^b)$ amount, as given by (115). This means that we can treat the right-hand side of (118) as a constant, and therefore that we need $b = 1$ to obtain a scaling appropriate to the outer problem.

We have now shown that the similarity between DEJ's results and those presented here is no coincidence. The inner problem close to the tip of the free surface is the same in each case, with the same underlying physics.

5. Conclusions

In this paper, we have shown that, although the problem of inviscid flow outside an initially wedge-shaped void has an obvious similarity scaling (Keller & Miksis 1983), no solution exists for sufficiently small wedge angles. The inclusion of an interior fluid inside the wedge only serves to decrease the range of angles for which a solution exists. Thus, there is no solution of the initial value problem for an inviscid fluid when the wedge semi-angle, α, is sufficiently small. The inclusion of the effect of viscosity at small times regularizes the problem when $t = 0^+$, and leads to a succession of pinch-off events, where a bubble of the interior fluid is detached when the free surface touches itself. We showed that asymptotic scalings exist for an inner region where this pinch-off event occurs, based upon the initial small wedge angle. Physically, the flow in the inner region is analogous to the pinch off of a constant-pressure region due to a uniform flow at infinity. Finally, we showed that these scalings are also consistent with the sequence of pinch offs that occur during the coalescnce of two inviscid spheres or cylinders, as described by Duchemin *et al.* (2003).

There are a number of issues related to this work that remain to be explored. Firstly, it would be worthwhile extending the unsteady numerical simulations presented here past the time where pinch-off occurs, both with no interior fluid and with a low-density interior fluid, to see whether there is a large difference in the dynamics, in particular the area of the bubble. Secondly, now that we have some idea of how to set up an inner asymptotic scaling, it should be possible to study the problem of the inviscid coalescence of two spheres or cylinders with non-zero initial approach velocity. Finally, the analagous problems of a slender wedge with an exterior void ($\rho = 0$, $\pi - \alpha \ll 1$) and a slender wedge with an exterior fluid of comparable density ($\rho = O(1)$, $\alpha \ll 1$) are also of interest, and it should be possible to tackle this using asymptotic methods analogous to those described by Decent & King (2001). Preliminary numerical results indicate that, in these cases, the tip of the wedge recoils through a distance of order $t^{2/3}\epsilon^{-1/3}$.

J. B. would like to thank the EPSRC for an Advanced Research Fellowship, which made this work possible. We would also like to thank Jean-Marc Vanden-Broeck for several helpful discussions.

REFERENCES

Billingham, J. 1999 Surface-tension-driven flow in fat fluid wedges and cones. *J. Fluid Mech.* **397**, 45.

Billingham, J. 2005 The initial, surface tension-driven flow of a wedge of viscous fluid. *SIAM J. Appl. Maths* (submitted).

Billingham, J. & King, A. C. 1995 The interaction of a moving fluid/fluid interface with a flat plate. *J. Fluid Mech.* **296**, 325.

Crapper, G. D. 1957 An exact solution for progressive capillary waves of arbitrary amplitude. *J. Fluid Mech.* **2**, 532.

Decent, S. P & King, A. C. 2001 The recoil of a broken liquid bridge. *Proc. IUTAM Symp. on Free Surface Flows* (ed. A. C. King & Y. D. Shikhmurzaev), p. 81. Kluwer.

Duchemin, E., Eggers, J. & Josserand, C. 2003 Inviscid coalescence of drops. *J. Fluid Mech.* **487**, 167 (referred to herein as DEJ).

Eggers, J. 1998 Coalescence of spheres by surface diffusion. *Phys. Rev. Lett.* **80**, 2634.

Eggers, J., Lister, J. R. & Stone, H. A. 1999 Coalescence of liquid drops. *J. Fluid Mech.* **401**, 293.

Keller, J. B. & Miksis, M. J. 1983 Surface tension driven flows. *SIAM J. Appl. Maths* **43**, 268.

Keller, J. B., Milewski, P. A. & Vanden-Broeck, J. 2000 Wetting and merging driven by surface tension. *Eur. J. Mech.* B – *Fluids* **19**, 491.

Keller, J. B., Milewski, P. A. & Vanden-Broeck, J. 2002 Breaking and merging of liquid sheets and filaments. *J. Engng Maths* **42**, 283.

King, A. C. 1991 Moving contact lines in slender fluid wedges. *Q. J. Mech. Appl. Maths* **44**, 173.

King, A. C., Billingham, J. & Popple, D. F. 1999 The moving contact line between two wedges of fluid on a flat plate. *Q. J. Mech. Appl. Maths* **53**, 453.

Lawrie, J. B. 1990 Surface tension driven flow in a wedge. *Q. J. Mech. Appl. Maths* **43**, 251.

Lawrie, J. B. & King, A. C. 1991 Exact solutions to a class of functional difference equations with application to a moving contact line flow. *Eur. J. Appl. Maths* **5**, 141.

Longuet-Higgins, M. S. & Cokelet, E. D. 1976 The deformation of steep surface waves on water I. A numerical method of computation. *Proc. R. Soc. Lond.* A **350**, 1.

Lundgren, T. S. & Mansour, N. N. 1988 Oscillations of drops in zero gravity with weak viscous effects. *J. Fluid Mech.* **194**, 479.

Sierou, A. & Lister, J. R. 2004 Self-similar recoil of inviscid drops. *Phys. Fluids* **15**, 1379.